Supplementary Information (SI) for Chemical Science.
This journal is © The Royal Society of Chemistry 2024

Supporting information

Phosphoester Bond Hydrolysis by a Discrete Zirconium-Oxo Cluster: Mechanistic Insights on a Central Role of Binuclear Zr^{IV}–Zr^{IV} Active Site

Edinara Luiz[a,b], Francisco de Azambuja[b*], Albert Solé-Daura[c*], Jordi Puiggalí-Jou[c], Angelo Mullaliu[b], Jorge J. Carbó[c], Fernando R. Xavier[d], Rosely A. Peralta[a*], Tatjana N. Parac-Vogt[b*]

[a] Departamento de Química, Universidade Federal de Santa Catarina, Florianópolis, Santa Catarina, 88040-900, Brazil.

[b] Department of Chemistry, KU Leuven, Celestijnenlaan 200F, 3001, Leuven, Belgium.

[c] Departament de Química Física i Inorgànica, Universitat Rovira i Virgili, Marcel·lí Domingo 1, Tarragona 43007, Spain.

[d] Departamento de Química, Universidade do Estado de Santa Catarina, Joinville, Santa Catarina, 89219-710, Brazil.

* tatjana.vogt@kuleuven.be; rosely.peralta@ufsc.br; francisco.deazambuja@kuleuven.be; albert.soled@urv.cat

Table of contents

1 General Remarks

All reactions were performed without any precautions against air and moisture. Unless otherwise noted, reagents were purchased from commercial sources, and used as received. All hydrolytic experiments were performed in duplicate or triplicate. Buffers HEPES (pH 7.0) and TRIS (pH 9.8) were prepared at 0.1 mol L^{-1} concentration using commercially available compounds in distilled water. The pH was corrected, under mild stirring, with KOH 1 mol L^{-1} using a conventional pH meter. For the reactions in deuterated water, pD was also measured in a conventional pH meter observing the relationship $pD = pH_{read} + 0.41$ to account for the isotopic composition of the solvent.[1] Deuterated HEPES buffer (0.1 mol L^{-1} - pD = 6.4) was prepared using HEPES and D_2O, and the desired pH_{read} was corrected with a commercially available NaOD 40% wt solution.

Materials

Carboxylic acid ligands acetic acid glacial, propionic acid, acrylic acid, butanoic acid, 2-methylbutanoic acid, methacrylic acid, benzoic acid and terephthalic acid, as well as (deuterated) solvents and buffer components were purchased from Fisher Scientific, Acros Organics or Sigma Aldrich. 1,3,6,8-tetrabromopyrene and 4-ethoxycarbonylphenylboronic acid were purchased from TCI. Ethyl paraoxon (diethyl-4-nitrophenylphosphate ≥ 90%), $ZrOCl_2.8H_2O$, $ZrCl_4$ and $Zr(OPr)_4$ 70 wt% were purchased from Sigma-Aldrich. Unless otherwise noted, all chemicals were purchased as pure reagent grades and used without further purification.

Preparation of known compounds

Zirconium oxo cluster catalysts were prepared according to previous literature reports: $[Zr_6O_4(OH)_4(OAc)_8(H_2O)(OH)Cl_3]$[2] (OAc = acetic acid) (**Zr_6**). The following clusters and MOFs were synthetized following previous literature reports: $[Zr_{12}(prop)]$[3] (prop = Propionic acid), $[Zr_{12}(OAcr)]$[4] (OAcr = acrylic acid), $[Zr_{12}(But)]$ [5] (But = butanoic acid), $[Zr_{12}(OAc)_{24}]$[3] (OAc = acetic acid), $[Zr_6$(2-MeBuCOO)][5] (2-MeBuCOO = 2-Methylbutanoic acid), $[Zr_6O_4(OH)_4(OMc)_{12}]$[6] (OMc = methacrylic

acid), $[Zr_6(BzO)_{12}]^7$ (BzO = benzoic acid). Zr-based metal-organic frameworks (Zr-MOFs) UiO-66 and NU-1000 were synthesized following methods used in our previous work.[8] The ligand tetraethyl-4,4′,4″,4‴-(pyrene-1,3,6,8-tetrayl)tetrabenzoate used in the synthesis of NU-1000 was prepared as described in our previous work.[9] All compounds presented satisfactory analysis coherent with characterization data published previously. All catalyst were dried under high-vacuum for at least 2 hours before use.

2 Experimental Procedures

2.1 Instrumentation

^{1}H NMR spectra were recorded on a Bruker Avance 400 spectrometer in deuterated water (D_2O – residual peak at 4.91 ppm) with 0.0016 mol L^{-1} of 3-(trimethylsilyl) propionic-2,2,3,3-d_4 acid sodium salt (TMSP-d_4) as an internal reference. Powder X-ray diffraction (PXRD) pattern was collected on a Malvern PANalytical Empyrean diffractometer (in transmission mode) over a 1.3 – 45° 2θ range, using a PIXcel3D solid state detector and Cu anode (Cu Kα1: 1.5406 Å; Cu Kα2: 1.5444 Å). Fourier-transform infrared spectra (FTIR) was recorded on a Bruker Vertex 70 spectrometer and analyzed with OriginLab software (version 8.5). Solid samples were measured directly, without sample preparation, using the attenuated total reflectance module (Platinum ATR). Kinetics studies were performed in a Agilent Cary 6000i UV-Vis-NIR spectrophotometer, in a quartz cuvette (optical path 1 cm), following the increase of 4-nitrophenol band at 317 nm (ε = 9021 L mol^{-1} cm^{-1}).

2.2 Cluster Digestion

12.0 mg of **Zr_6** cluster was dissolved in 700 μL of NaOD 1 mol L^{-1}. After 24 h, the sample was centrifugated for 3 minutes at 15000 rpm. 600 μL of the supernatant solution was transferred to an NMR tube with 15 μL of a TMSP-d_4 0.055 mol L^{-1} solution, and the ^{1}H NMR of this sample was measured in a 400 MHz Bruker Avance spectrometer.

*2.3 Hydrolysis reaction of **1** using $ZrCl_4$ or ZrO_2*

For the experiments using $ZrCl_4$ as a catalyst, Zr salt was added using stock solutions of $ZrCl_4$ in water or HEPES buffer. For the reactions in water, 600 μL (1.5 μmol of Zr) of $ZrCl_4$ stock solution (2.57×10^{-3} mol L^{-1} of Zr) were diluted in 400 μL of water. For the reaction in HEPES buffer, 200 μL of $ZrCl_4$ stock solution (9.40×10^{-3} mol L^{-1} of Zr) (1.5 μmol) were diluted 800 μL of buffer (HEPES 0.1 mol L^{-1} pH= 7.0). The reactions were carried out and monitored as described for **Zr_6** for 31 h at 60 ˚C and pH values reported were measured before and after the reaction. The same procedure was used for the reactions carried out using ZrO_2, but the catalyst was added directly as a solid due to its heterogeneous nature.

2.4 Potentiometric titration

Titration was performed in a Mettler-Toledo T5automatic titrator. Calibration was performed with commercial buffers of pH 2.00, 4.00, 7.00, and 12.00 (Chem Lab). **Zr_6** (52 mg) and KCl (29 mg) were diluted in water (40 mL). The solution was covered with parafilm and allowed to equilibrate for 2h prior titration. The initial pH was measured, and then titrated with a commercially available KOH 0.1 mol L^{-1} aqueous solution (standardized before analysis) until pH 11.5. The injection volumes ranged between 0.05 mL and 0.005 mL. The titration curves were measured for two samples, with less than 3% variation between runs. Equivalence points were calculated using the first derivative of curves following the pH variation as a function of titrant added volume. The derivative maximum points indicate the equivalence points. The pK_a values were determined as the pH of solution when one-half of the volume of titrant need to reach an equivalence point had been added, as previously reported in the literature.[10]

2.5 EXAFS analysis

X-ray absorption fine structure (XAFS) spectroscopy experiments were performed at the XAFS 11.1 beamline of Elettra - Sincrotrone Trieste (Italy).[11] The storage ring operated at 2.4 GeV in top-up mode with a typical current of 310 mA. XAFS data were recorded at the Zr K-edge in transmission mode

using pellets made upon mixing a proper amount of Zr-based cluster and cellulose. Spectra were acquired from 17698 eV to 19522 eV around the Zr K-edge with a constant k-step of 0.03 Å-1 and 2 s/point acquisition time.

The extended XAFS (EXAFS) analysis was performed using the GNXAS package[12,13] based on the multiple scattering (MS) theory. The sinusoidal signal of the experimental EXAFS spectra was described by considering only a few key contributions from the structural model shown in **Scheme S1**. Two two-body ($\gamma^{(2)}$) terms were used to account for the two different structural oxygens in the Zr first-shell environment ($\gamma_1^{(2)}(Zr-O1)$ and $\gamma_2^{(2)}(Zr-O2)$, each with degeneracy $N = 4$), while two additional two-body signals were used to describe the Zr--Zr pairs ($\gamma_3^{(2)}(Zr-Zr)$ with $N = 4$ and $\gamma_4^{(2)}(Zr-Zr)$ wit $N = 1$).

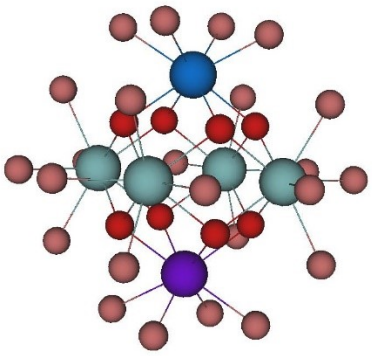

Scheme S1. Graphical representation of the structural model used for the EXAFS analysis. Each Zr (for instance, blue Zr on top) sees eight oxygens ($4\mu_3$-O ~2.1 Å and $4\mu_2$-O ~2.2 Å, described by γ_1 and γ_2, respectively), four equatorial Zr atoms (light blue atoms at ~3.6 Å, included in γ_3) and one apical Zr (violet atom at ~5.0 Å, γ_4).

3 Results and Discussion

3.1 Zr_6 characterization

PXRD pattern is similar to previous reported.[2] In the IR spectra it is possible to observe the symmetric and asymmetric bands for the coordinated acetate ligands at in 1457 and 1547 cm^{-1}, respectively. In addition, the Zr-O stretch in 649 cm^{-1}, and water (O-H) band in 3270 cm^{-1}, both bounded to Zr.

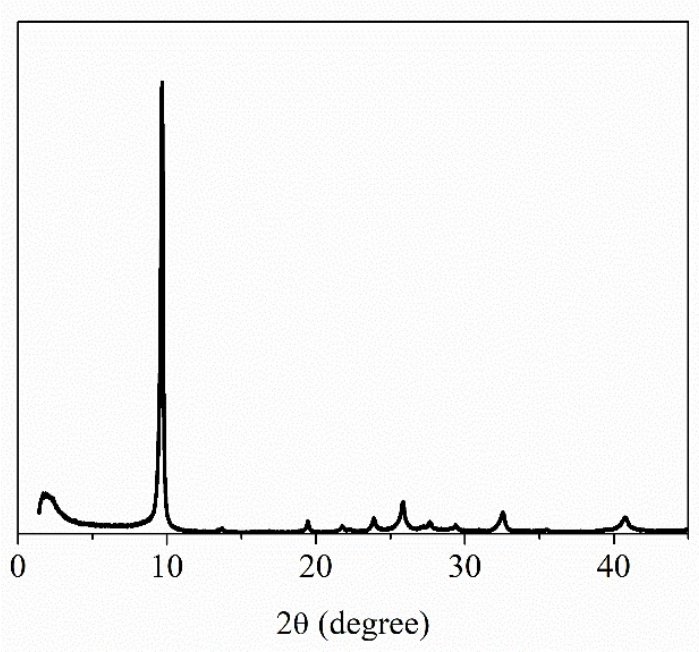

Figure S1. Experimental PXRD pattern of the **Zr_6** cluster.

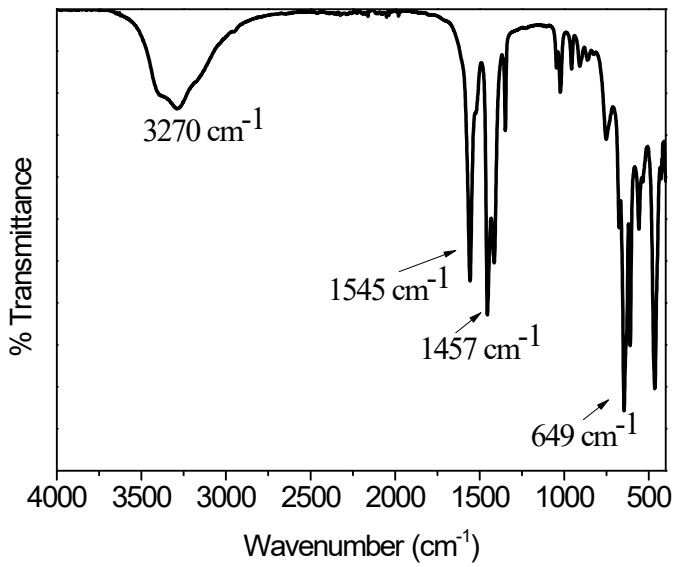

Figure S2. Infrared spectrum of the as-synthesized **Zr_6** Cluster.

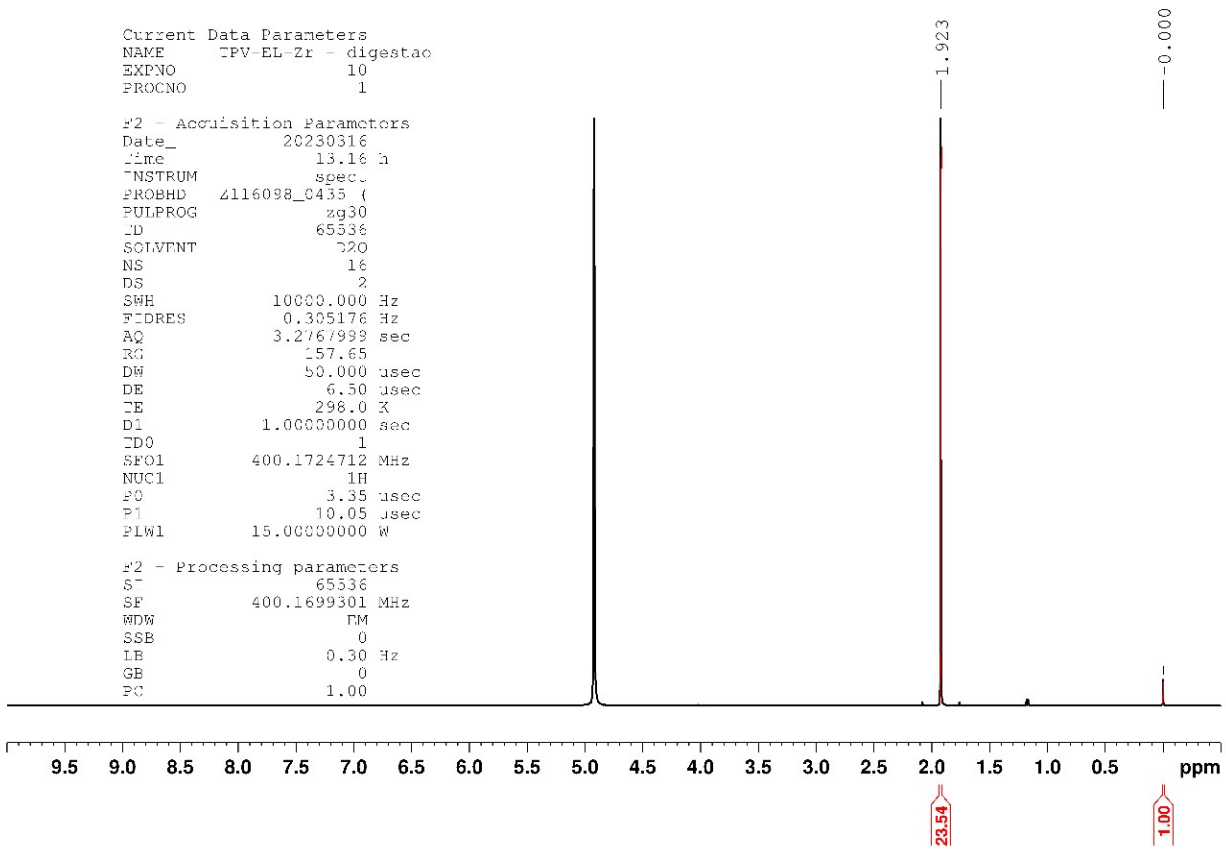

Figure S3. [1] H NMR of **Zr_6** cluster digested in NaOD 1 mol L^{-1}. [1]H NMR spectra, 400 MHz in D_2O, $\delta = 0.00$, TMSP-d_4 0.0016 mol L^{-1}; $\delta = 4.93$, HDO.

3.2 Hydrolytic experiments

1) Screening reactions were performed by ^{1}H NMR analysis in different conditions of temperature (25, 37 or 60 °C) and pH (3.0, 6.4 or 9.0), using 6 mol% catalyst and deuterated water or buffer solution (HEPES 0.1 mol L^{-1} for pH 7.0 and TRIS 0.1 mol L^{-1}dor pH 9). The reactivity was evaluated by looking into the ratio of product/substrate after 24 h of reaction. This ratio was determined by integration of substrate **1** and corresponding product peaks, as exemplified in **Figure S4**.

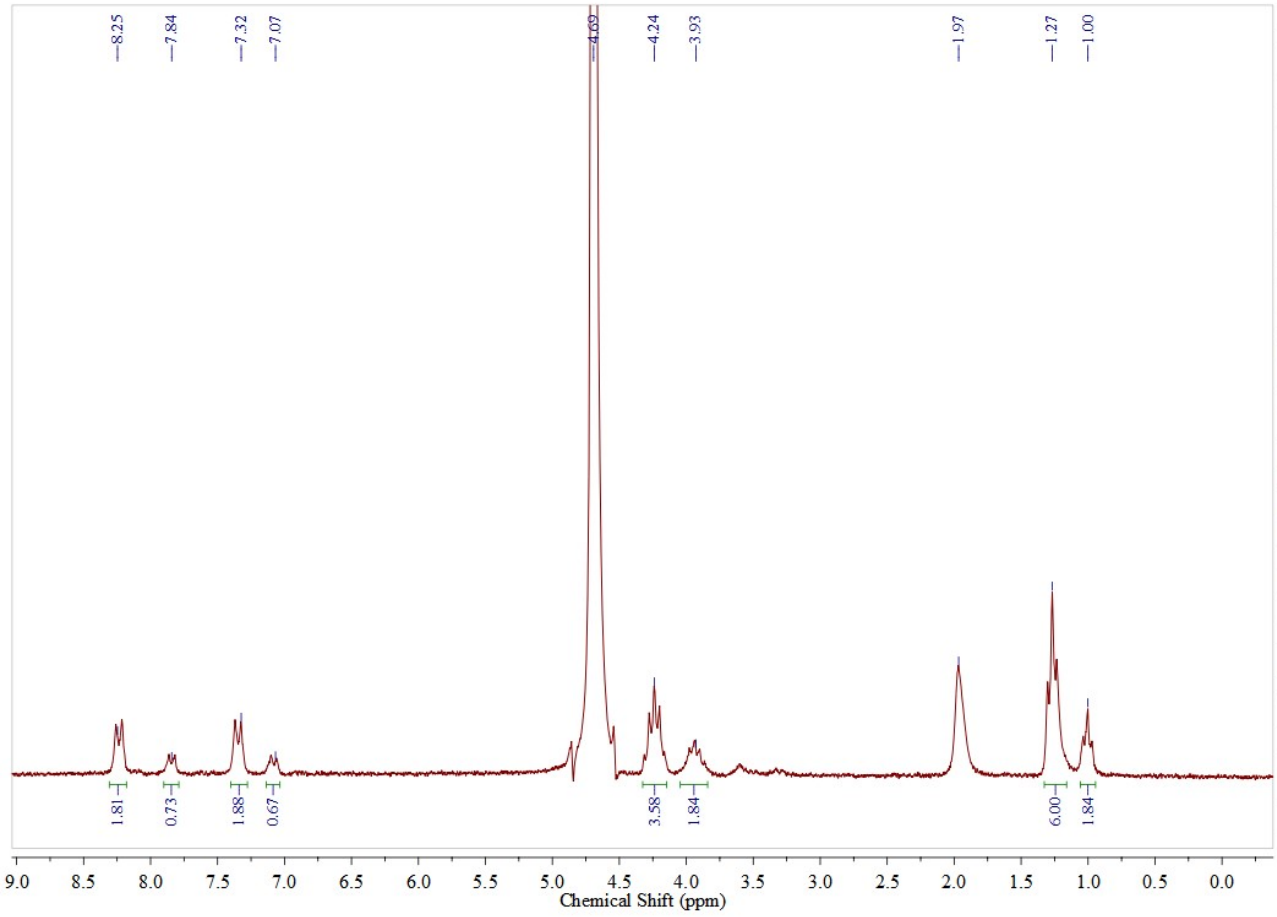

Figure S4. ^{1}H NMR spectra, 400 MHz in D_2O, of **Zr_6** catalyzed hydrolysis of (**1**). Conditions: [**Zr_6**] = 1.5 mmol L^{-1}; [**1**]= 25 mmol L^{-1}, 600 µL, at 37ºC. Peaks referent to (**1**): δ (ppm) 8.25; 7.32; 4.24; 1.27. Peaks referent to products, in ppm: 7.84; 7.07; 3.93; 1.00. δ = 4.69, HDO; δ = 1.97, Acetate.

2) Hydrolytic reactions were followed by monitoring the concentration of 4-nitrophenol (4-NP) product band in UV-Vis spectroscopy. To establish the concentration of product released, the molar absorption coefficient (ε) was determined using commercially available 4-NP (**Figure S5**). By measuring the UV/Vis spectra of different concentrations of 4-NP in water (acidic pH), and using Lambert-Beer law (Equation 1), the ε was determined to be 9021 L mol^{-1} cm^{-1} at 317 nm.

Equation 1 $$A = b.C.\varepsilon$$

Where A is absorbance, C is concentration, b is optical path, which is one centimeter in this case.

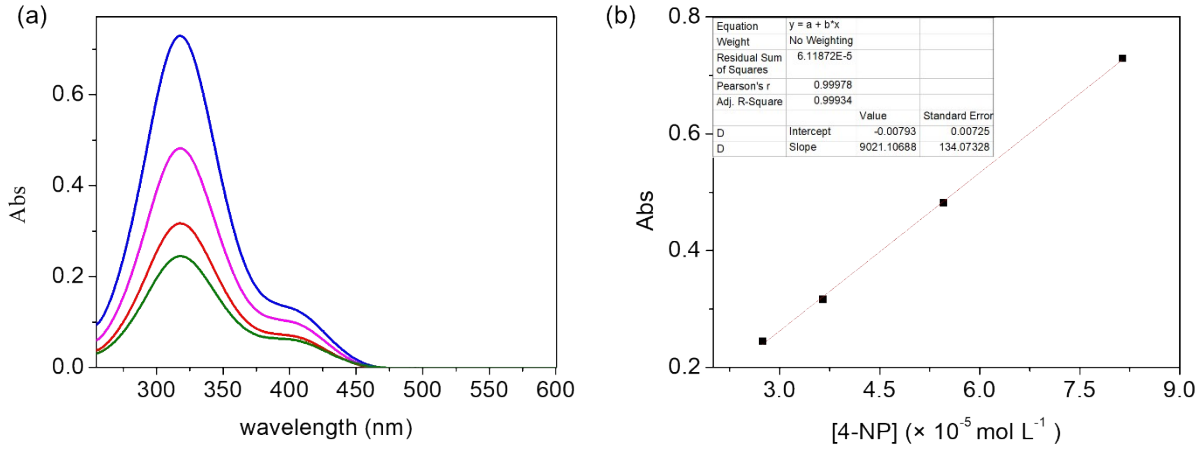

Figure S5. UV-Vis analysis (a) and molar absorption coefficient determination at 317 nm (b) of 4-NP in water (pH 3.0 corrected with HCl, 1 mol L^{-1}). [4-NP] = 2.75×10^{-5} to 8.15×10^{-5} mol L^{-1}.

3) NMR analysis of the main reactions were performed to confirm the presence of products after 24h reaction. The respective spectra are presented below.

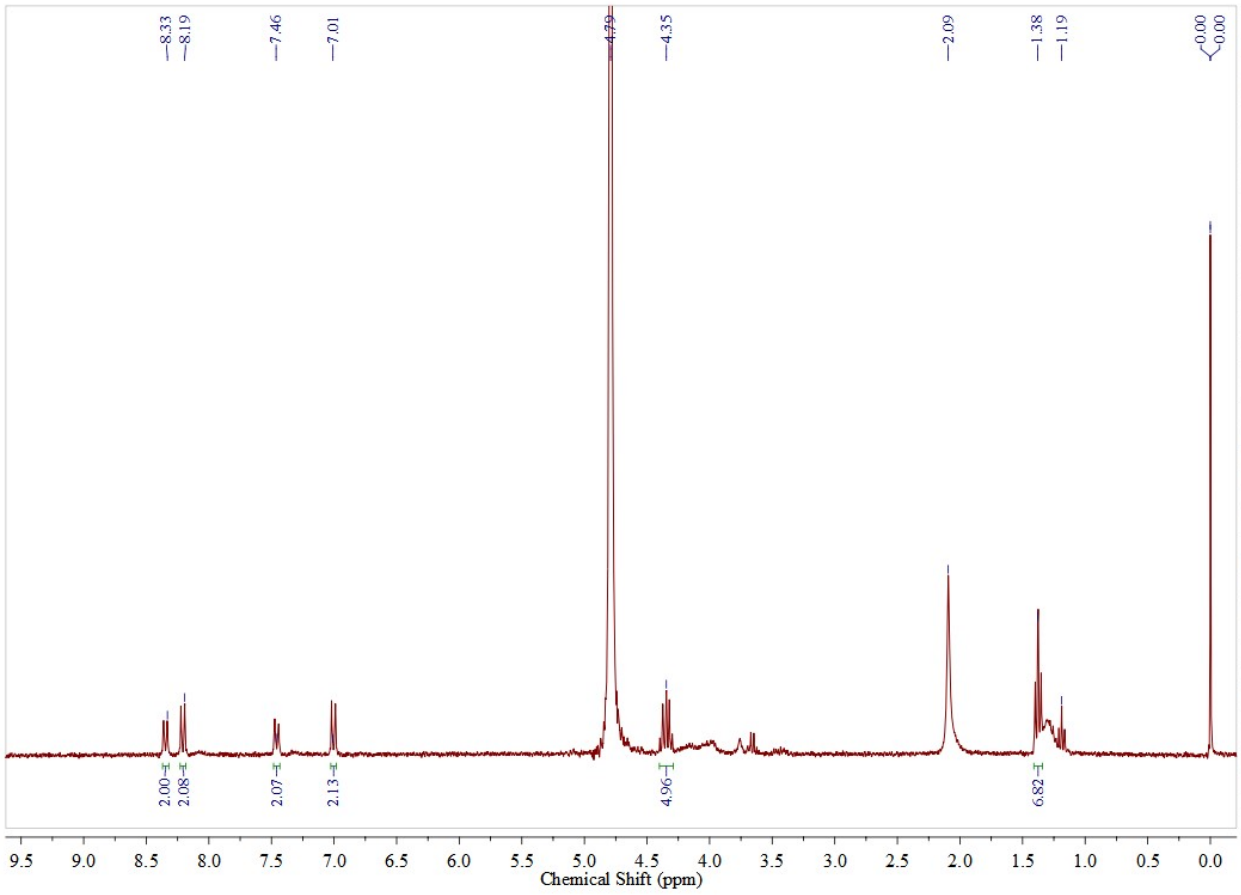

Figure S6. ^{1}H NMR (400 MHz) of reaction at pH 3.0 in D_2O. Peaks attribution (in ppm): δ = 0.00, TMSP-d_4 0.0016 mol L^{-1}; δ = 4.93, HDO; δ = 2.09, Acetate; δ = 8.33, 7.46, 4.35, 1.38, refer to **1**; δ = 8.18, 7.01, 1.19, refer to products.

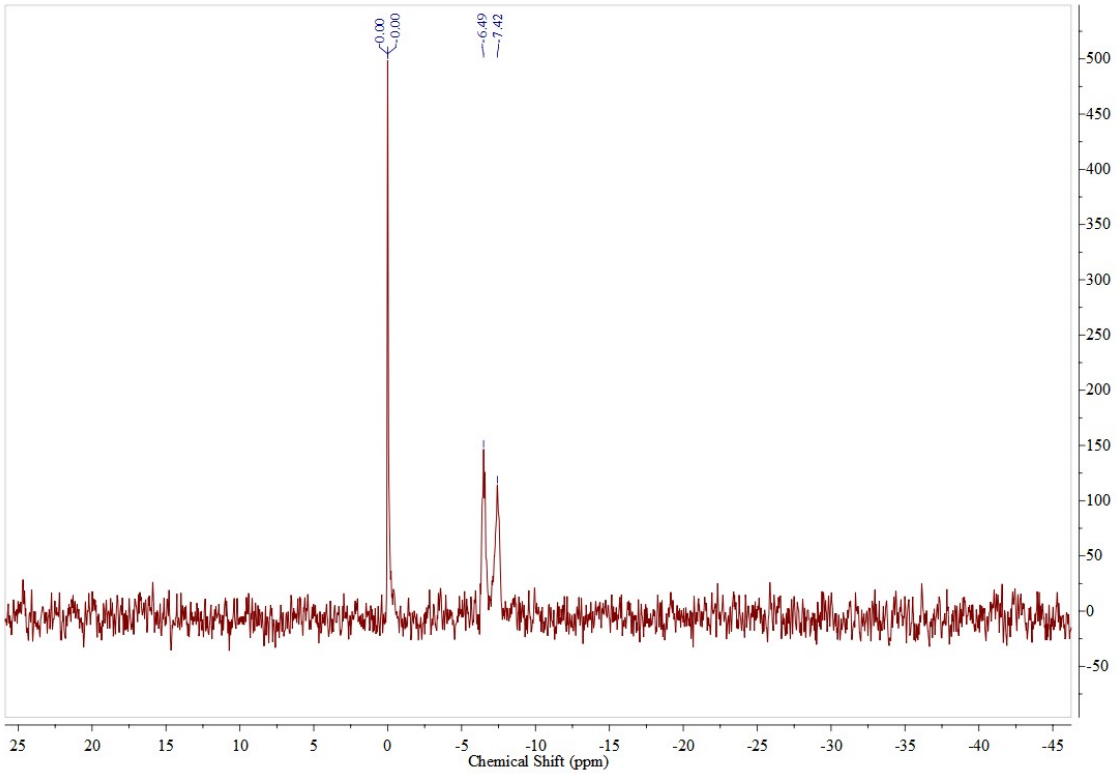

Figure S7. ^{31}P NMR (180 MHz) of reaction at pH 3.0, in D_2O. Peaks attribution (in ppm): δ = 0.00, H_3PO_4; δ = 6.49, refers to **1**. δ = 7.42, refer to product.

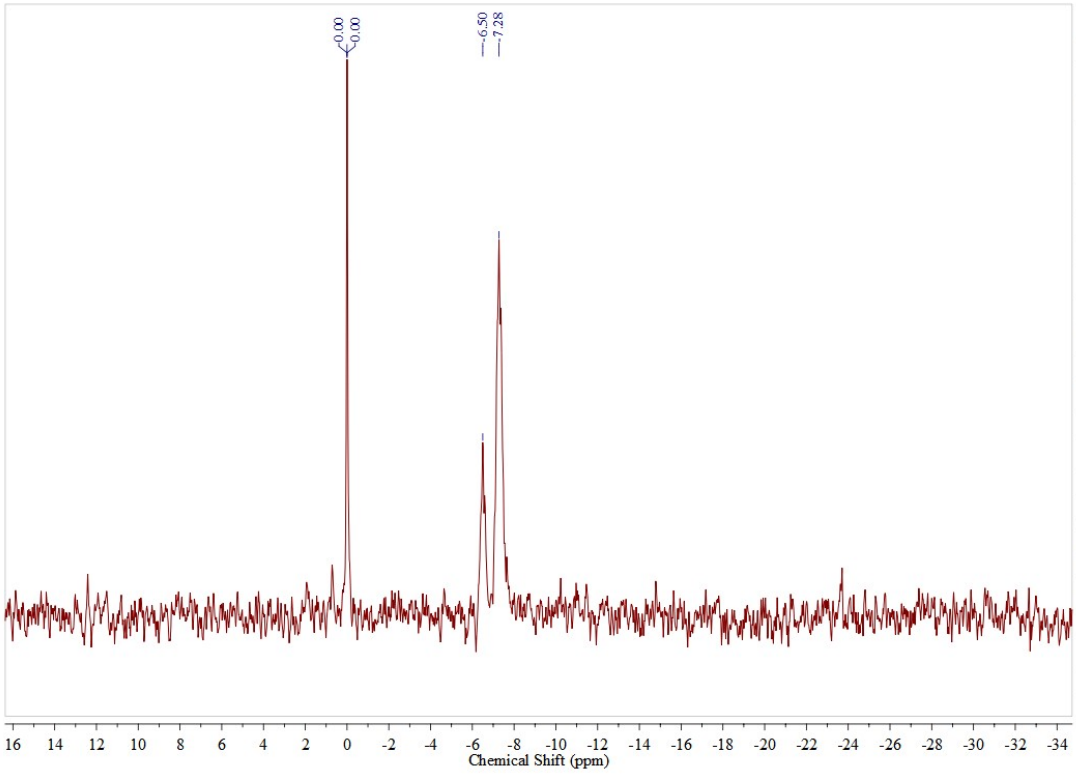

Figure S8. ^{31}P NMR (180 MHz) of reaction at pH 6.4, in D_2O (HEPES pH 7.0, 0.1 mol L^{-1}). Peaks attribution (in ppm): δ = 0.00, H_3PO_4; δ = 6.50, refers to **1**. δ = 7.28, refer to product.

4) The buffer effect was analyzed using different buffers at the same pH and concentrations. The organic buffers HEPES and Bis-TRIS and the inorganic carbonate/bicarbonate were prepared as 0.1 mol L^{-1} solutions at pH 7.0. The hydrolysis reaction conducted at 60ºC in the same conditions described in the main text. Both catalyzed and uncatalyzed reactions were conducted. Although the yields generated by HEPES and carbonate/bicarbonate buffers is similar after 24 h reaction, the inorganic buffer affords a similar yield in the absence of catalyst. This is in line with the susceptibility of the substrate **1** to the presence of nucleophilic bases (Figure 1c of the main text), and the likely low stability of $\mathbf{Zr_6}$ cluster in carbonate solution reported previously.[14] Thus, the hydrolysis in this case is mostly related to the buffer than the cluster itself, unlike for the reaction in HEPES buffer solution. Comparing the three reaction conditionss, the Bis-TRIS buffer generates the best yield after 24 h. This reaction even surpassed the ~20% yield of other reactions, suggesting that Bis-TRIS is a good option for these reactions. Nevertheless, reactions in HEPES are faster as observed by comparing the 5 h results.

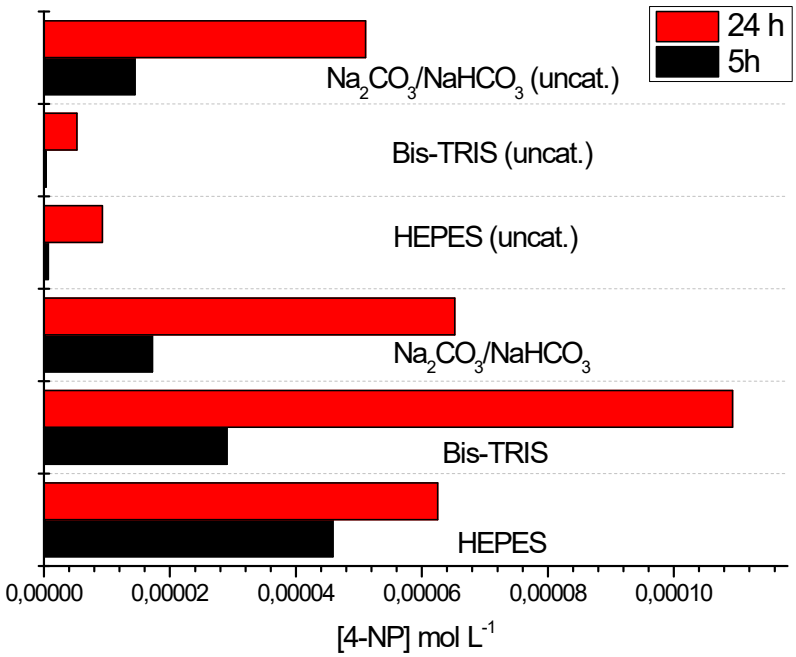

Figure S9. Hydrolysis of **1** at different buffers at pH 7.0, with and without $\mathbf{Zr_6}$ as catalyst. Conditions: [$\mathbf{Zr_6}$] = 1.5 mmol L^{-1}; [**1**]= 25 mmol L^{-1}; solvent HEPES, Bis-TRIS or carbonate/bicarbonate 0.1 mol L^{-1} (pH 6.4 - 6.7)), 60 ºC.

5) Under acidic conditions, no beneficial effect of using $ZrCl_4$ as catalyst was observed (similar conversion to the uncatalyzed one). In addition, $ZrCl_4$ behaved the same during the first hours of reactions conducted in acidic or 'neutral' (pH 6.7) conditions, though later $ZrCl_4$ activity gradually increases in pH 6.7. This distinct behavior could be potentially linked to the aqueous chemistry of Zr^{IV} cations.[15] When $ZrCl_4$ is dissolved in water, it promptly hydrolyzes forming $[Zr_4(OH)_8(OH_2)_{16}]^{8+}$ tetramers similar to **Zr_6**, the water ligands of this cluster can deprotonated in solution, generating a more acid environment. Accordingly, reactions using $ZrCl_4$ in water presented an initial pH = 2.7, whereas pH = 6.7 in HEPES buffer. More extensive hydrolysis of $ZrCl_4$, and/or further re-structuring of tetramers into more active species could be causing the reaction to be faster at pH 6.7 than at pH 2.7 as time passes.

ZrO_2 was also tested as catalyst in the same conditions described above. Its poor solubility in water likely contributes to the low conversion of **1** into products. No effect of ZrO_2 was observed when the reaction was performed in HEPES buffer (pH 7.0, 0.1 mol L^{-1}), while minimal catalytic activity was observed for the reaction conducted in water. The slightly better outcome for the reaction conducted in water using ZrO_2 in comparison to the one using $ZrCl_4$ might be due to the pH of the ZrO_2 reaction (~ 6.0 vs 2.7 for $ZrCl_4$), where reactions were usually better, as previously discussed.

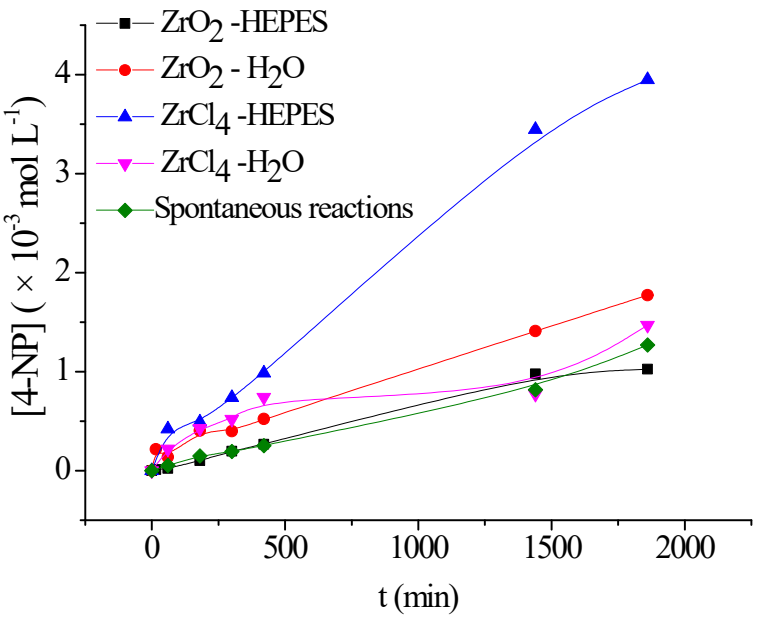

Figure S10. Zr salts (ZrO_2 and $ZrCl_4$) catalyzes hydrolysis of **1** at 60 °C in pH 3.0 (ZrO_2 - red circles ●; $ZrCl_4$ – pink triangles ▼) and 6.4 (ZrO_2 – black squares ■; $ZrCl_4$ – blue triangles ▲). Spontaneous hydrolysis in both pH 7.0 (HEPES 0.1 mol L^{-1}) and pH 3.0 are presented by green squares (♦). Conditions: [$ZrCl_4$] = [ZrO_2] = 1.5 mmol L^{-1}; [**1**]= 25 mmol L^{-1} l; solvent (1 mL – water (pH 2.7 - 3.0) or HEPES 0.1 mol L^{-1} (pH 6.4 - 6.7)), 60 ºC.

6) The observed initial rate constants (k_{obs}) were obtained by fitting the 4-NP (**3**) concentration over time to first order reaction equations (**Figure S11**). The reactions performed using **Zr_6** as catalyst do not fit neither pseudo first-order nor second-order kinetics, due to the partial inhibition of catalyst by diethylphosphonic acid (**2**).[16] Thus, the first-order equation was applied until the first 5-7 h, until less than 10% conversion, when the inhibition effect is negligible.

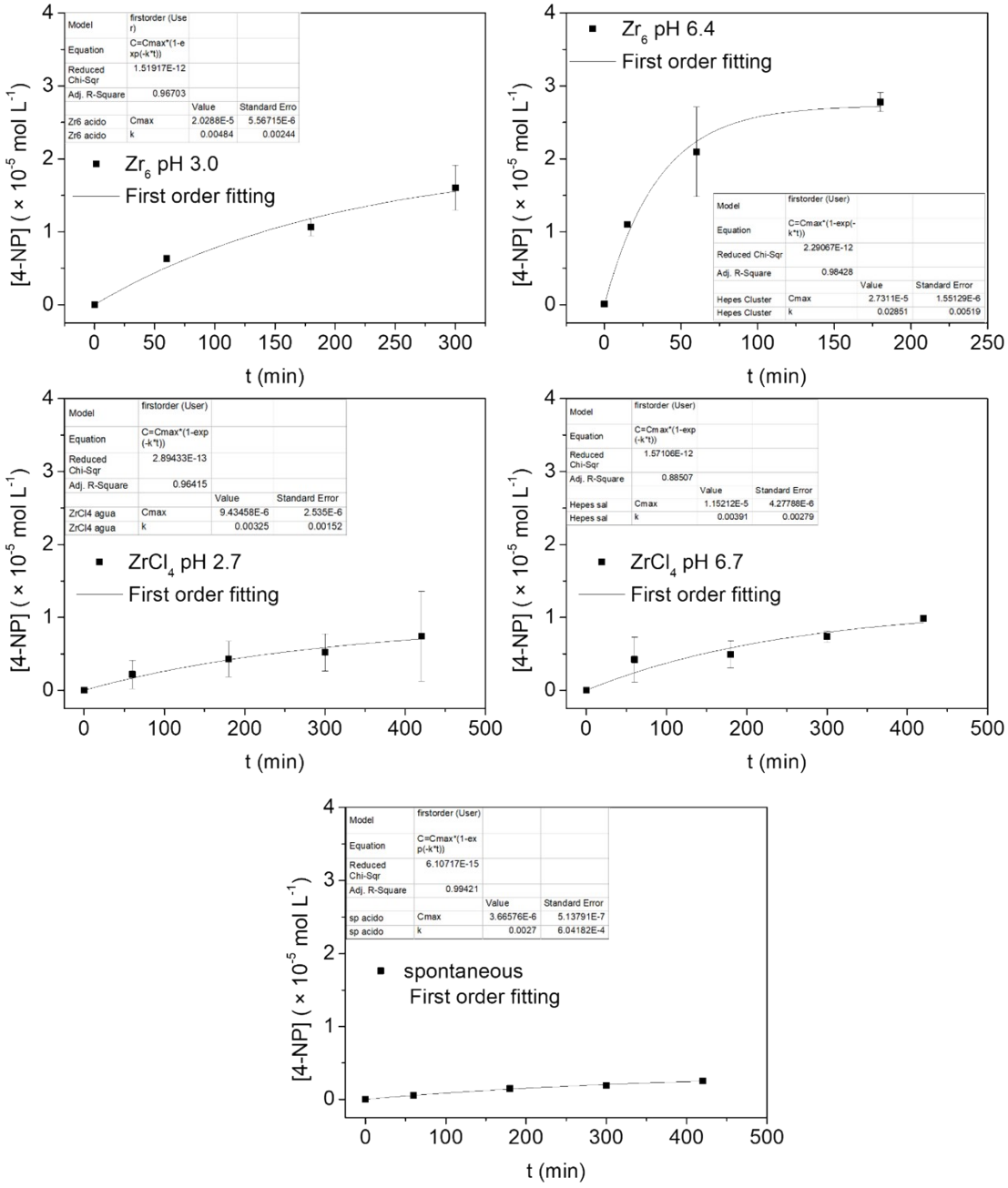

Figure S11. First order fitting for catalyzed reactions and spontaneous hydrolysis. [Zr_6] = [$ZrCl_4$] = 1.5 mmol L^{-1}; [**1**] = 25 mmol L^{-1}; 60ºC; in water and HEPES (0.1 mol L^{-1} – pH 7.0). Spontaneous hydrolysis profile do not change in the different conditions tested.

7) Reported results for others catalysts used in the hydrolysis of **1**

Even though PAPs normally require a heterovalent binuclear core, several structural mimetics prove to be efficient even with binuclear bivalent metals.[17] However, in these cases is normally necessary to increase the pH in order to obtain the catalytic species. With Zr^{IV} cluster is possible to achieve the catalytic species in an even more acidic pH, more similar to the natural enzymatic environment than for mimetic compounds previously reported. Besides, using homogeneous inorganic catalysts to cleavage toxic organophosphates is, as the best of our knowledge, one poorly explored field. A comparison of our results with other coordination compounds reported previously evidences the promising potential of Zr oxo cluster catalysts (**Table S1**).

Table S1. Comparison between reported homogeneous catalysts for the hydrolysis of **1**. Catalytic constants to Zr_6 were converted from min^{-1} to s^{-1} to ease the comparison.

Catalyst	pH	k ($\times 10^{-5}$ s^{-1})
$\mathbf{Zr_6(OAc)_8}$	3.0	8.00
$\mathbf{Zr_6(OAc)_8}$	6.4	46.60[a]
$\mathbf{Zn^{2+}}$**–[12]aneN**[18]	8.1	1.01[b]
$\mathbf{[Zn_2(HL_1)_2(Py)_4].2H_2O}$[19]	8.5	0.25[c]
$\mathbf{[Zn_2(H_2L_3)_2(NO_3)_2]}$[19]	8.5	0.40[c]

[a]This work; [b]in 50% H_2O, 37.5% D_2O, and 12.5% CD_3CN at 50 °C, [12]aneN = 1,4,7,10-tetraazacyclododecane; [c]in DMSO/buffered H_2O (1:1) at 50 °C, HL_1= 3-[(1*E*)-*N*-hydroxyethanimidoyl]-4-methyl-1*H*-pyrazole-5-carboxylic acid, py = pyridine, H_2L_3 = (*E*,*E*)-(4- methyl-1*H*-pyrazole-3,5-diyl)bis(methylmethanone) dioxime.

3.3 Analysis of Zr_6 after reaction

1) The **Zr_6** was recovered after reaction by centrifugation (15000 rpm for 3 min) and washed with 2 times of acetone (1 mL for 5 min each time). After drying at room temperature for one day, the precipitate was analysed by IR, NMR (after digestion with 1 mol L^{-1} NaOD)[20] and EXAFS. The IR spectra and NMR show acetate capping ligands are present, suggesting that some of them remain bound to the cluster after reaction in both conditions.

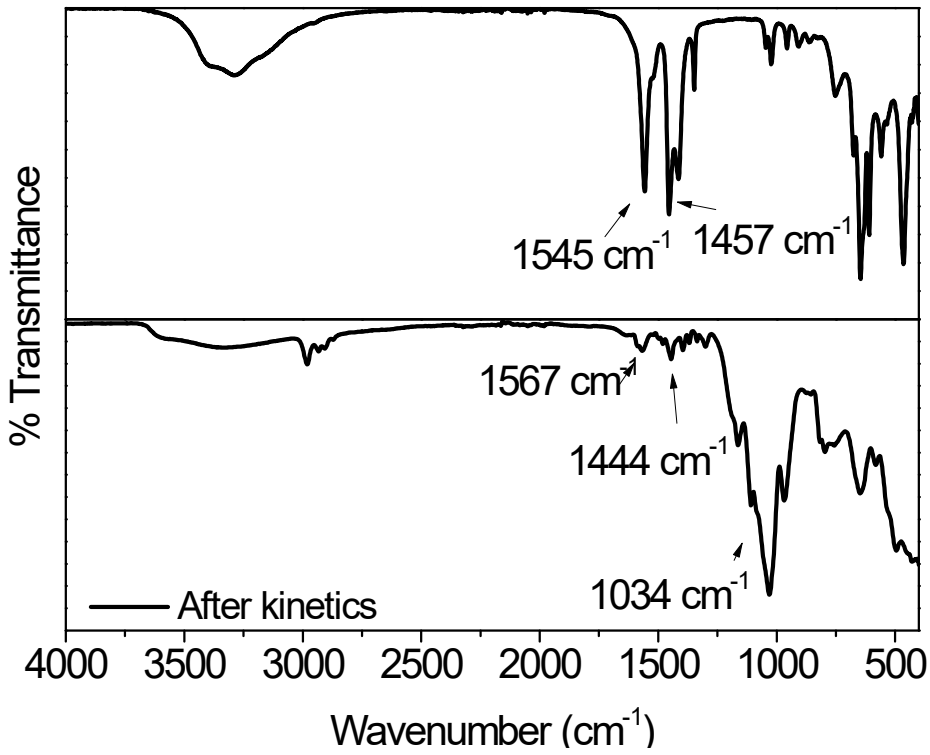

Figure S12. Infrared spectra of the as-synthesized **Zr_6** cluster (top), and precipitate collected after reaction, in pH 6.4 (bottom).

(a)

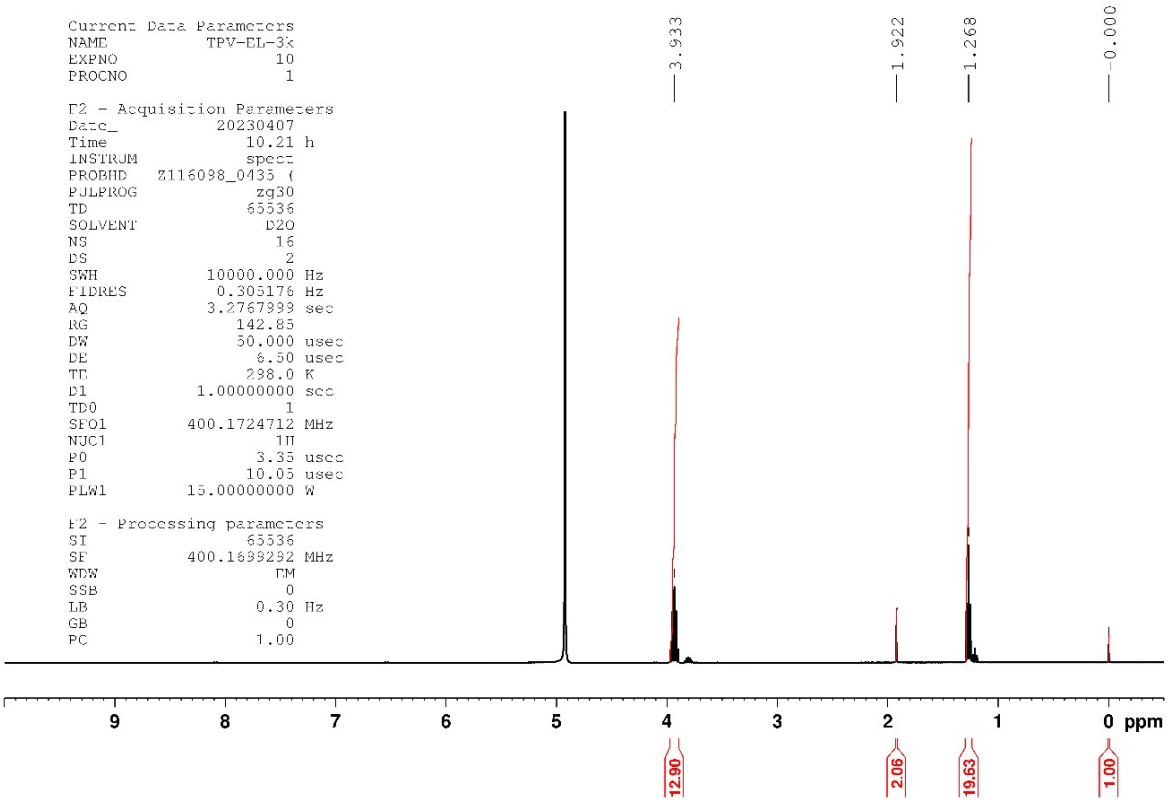

(b)

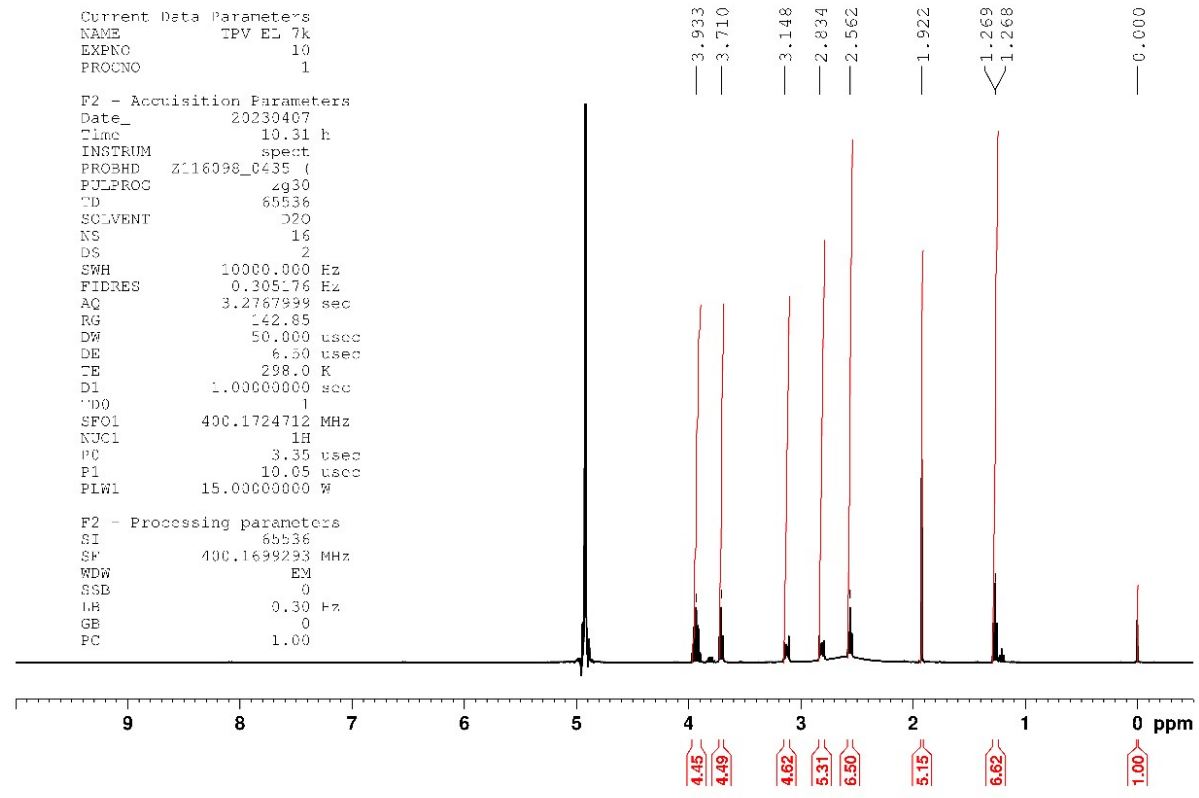

Figure S13. ^{1}H NMR of precipitate after reaction (a) at pH 3.0 (b) at pH 6.4, digested in NaOD 1 mol L^{-1}, ^{1}H NMR spectra, 400 MHz in D_2O, δ = 0.00, TMSP-d_4 0.0016 mol L^{-1}; δ = 4.93, HDO; δ = 1.92, Acetate. Buffer (δ, in ppm): 2.56, 2.83, 3.15, 3.71.

2) EXAFS spectra were analyzed after exposure to pH = 3 and pH = 6.4. The extracted EXAFS signals (**Figure S14a-b**) and respective Fourier transforms (FTs) (**Figure S14c-d**) highlight a good match between experimental and calculated signals. By taking a closer look at the FTs, the second peak, which correlates to the second-shell coordination (Zr--Zr), decreases at pH = 6.4. This is reflected in the decrease in the γ_3 path degeneracy, as shown in **Table S3** (from 4.0 to 3.6). However, retrieved structural parameters are statistically equivalent as their error bars overlap, suggesting that the cluster at the two pH values is not significantly different. Further evidence of having a cluster in both conditions is also the presence of the contribution at ~4.7 Å in the FTs, which was fitted by considering the Zr--Zr scattering of opposite Zr atoms (γ_4).

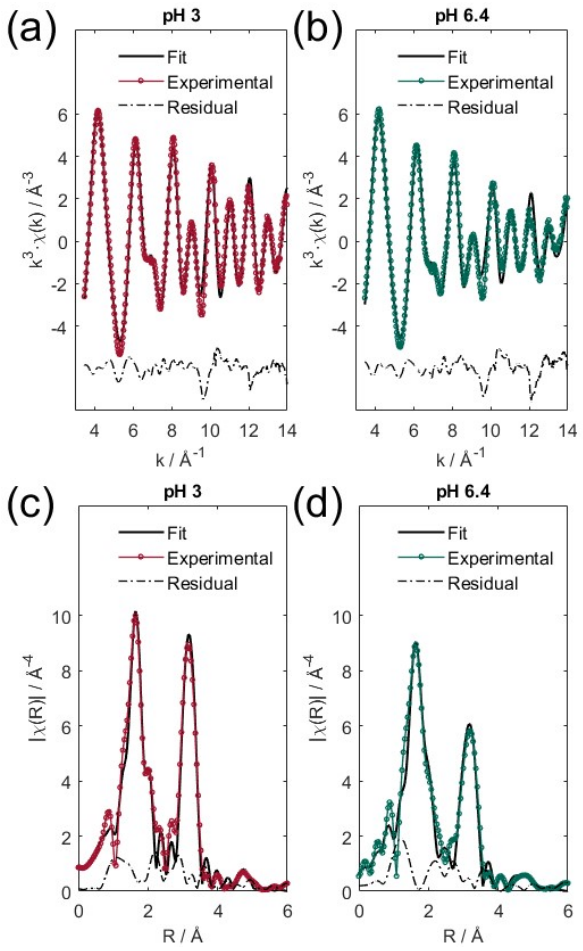

Figure S14. EXAFS best fit for samples at **(a)** pH = 3.0 and **(b)** pH = 7.0 and respective **(c,d)** Fourier transforms (FTs). The experimental signals are compared to the calculated ones, highlighting a good match between the experimental structure and adopted model.

Table S2. Relevant EXAFS retrieved parameters at pH = 3.0 and pH = 6.4. Interatomic distances (**R**), Debye-Waller factors (**σ²**), and signal degeneracies (**N**) are reported with the respective errors in brackets. No significant difference is appreciated in the two conditions, as the error bars for each structural parameter overlap.

		pH = 3.0	**pH = 6.4**
$\gamma_1^{(2)}\,(Zr-O)$	**R / Å**	2.148(12)	2.160(10)
	σ² / Å²	0.007(2)	0.007(2)
	N	4.0(4)	4.0(4)
$\gamma_2^{(2)}\,(Zr-O)$	**R / Å**	2.226(12)	2.213(13)
	σ² / Å²	0.008(2)	0.011(3)
	N	4.0(6)	4.0(6)
$\gamma_3^{(2)}\,(Zr-Zr)$	**R / Å**	3.63(2)	3.63(2)
	σ² / Å²	0.010(2)	0.012(3)
	N	4.0(8)	3.6(9)

3) Reactions using the recovered cluster were performed in water at 60ºC for 24h. In this reaction, the solution acidification after addition of cluster as in its first use was not so intense, the reaction initial pH was circa 5.0. However, the final pH also decreased to 1.80 after the 24h. A control experiment was performed dissolving only recovered **Zr_6** (2.0 mg) in HEPES (0.1 mol L^{-1} - pH 7.0) to ensure that any product observed in the recycling experiment is not due to **1** adsorbed to the catalyst carried through from the first reaction.

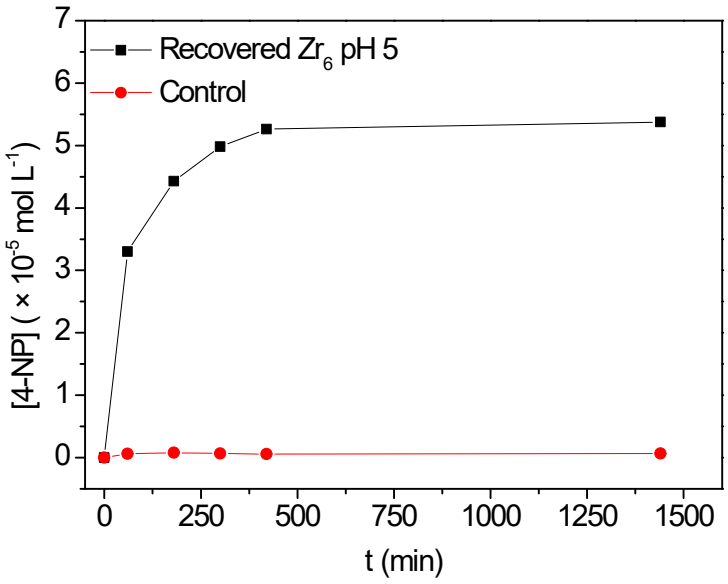

Figure S15. Hydrolysis of **1** using recovered **Zr_6** cluster. Conditions: [Zr_6] = 1.5 μmol; [**1**] = 25 μmol; solvent (1 mL – water pH 5.0), 60 ºC.

Acidification to pH 3.0 when using the recovered **Zr_6** cluster did not happen because the exchange of phosphate **2** bound to the used cluster by water in solution did not afford the same acidification derived from the deprotonation of water coordinated to Zr in the first reaction. This is self-evident from the pK_a values estimated for the cluster in Figure 6 of the manuscript (3.80, 4.76 and 6.43) and the pK_a of phosphate product **2** (1.42), which show that in the presence of **2**, the equilibrium disfavors the dissociation of water molecules coordinated to the cluster, consequently resulting in a much lower acidification of the reaction medium. We refrained to acidify the reaction using external acids to avoid any undue interferences in the reaction kinetics. Nevertheless, considering the evidence of cluster integrity during the reaction (EXAFS analysis, **Table S2**), the likely acid-base equilibria present in the reaction medium and the identical acidification to pH 1.80 at the end of reaction as observed for the first reaction cycle, it becomes clear that the recycling experiment is representative, despite of not exhibiting the same acidity at the beginning of the reaction. Remarkably, this independence with respect to the acidity also corroborates the role of **Zr_6** as a Lewis acid catalyst elucidated in our DFT study.

3.4 Hydrolysis using Zr-MOF and other clusters

Table S 3. Different Zr_6 and Zr_{12} clusters probed as catalysts for the hydrolysis of **1**, yield of 4-NP (**3**), and pH of reaction solution at the beginning of reaction, and after 24 h.[a]

Cluster	Ligand	Yield (%) (24h)	pH_i	pH_f
Zr_{12}(prop)^3	Propionic acid	18	4.1	2.0
Zr_{12}(OAcr)^4	Acrylic acid	19	3.7	2.0
Zr_{12}(But)^5	Butanoic acid	18	3.7	2.0
$Zr_{12}(OAc)_{24}$^{3}	Acetic acid	19	3.9	2.0
Zr_6(2-MeBuCOO)^5	2-Methylbutanoic acid	19	4.1	2.0
$Zr_6(OMc)_{12}$ ^{6}	Methacrylic acid	18	4.0	1.7
$Zr_6(BzO)_{12}$^{7}	Benzoic acid	13	3.5	2.4

[a] Conditions: [Zr]= 1.5 µmol; [**1**]= 25 µmol, water (1 mL), 60 ºC.

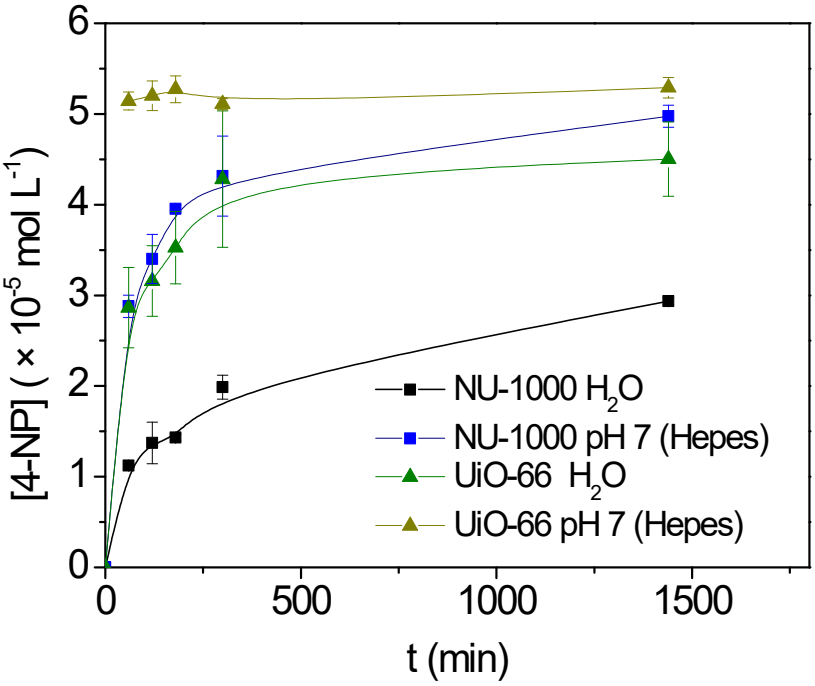

Figure S16. Catalyzed hydrolysis of **1** by Zr-MOF in HEPES and water. Conditions: [MOF] = 1.5 µmol; [**1**] = 25 µmol; 60ºC; in water (1 mL, pH 4.0); and HEPES 0.1 mol L^{-1} (1 mL, pH 7.0).

In basic conditions, a decrease in pH before and during reaction has also been observed. After 24h reaction, the pH dropped from 8.9 to 7.8 and from 9.1 to 8.1 using Zr-cluster and UiO-66 respectively. The spontaneous hydrolysis in this condition was circa 6% after 24h.

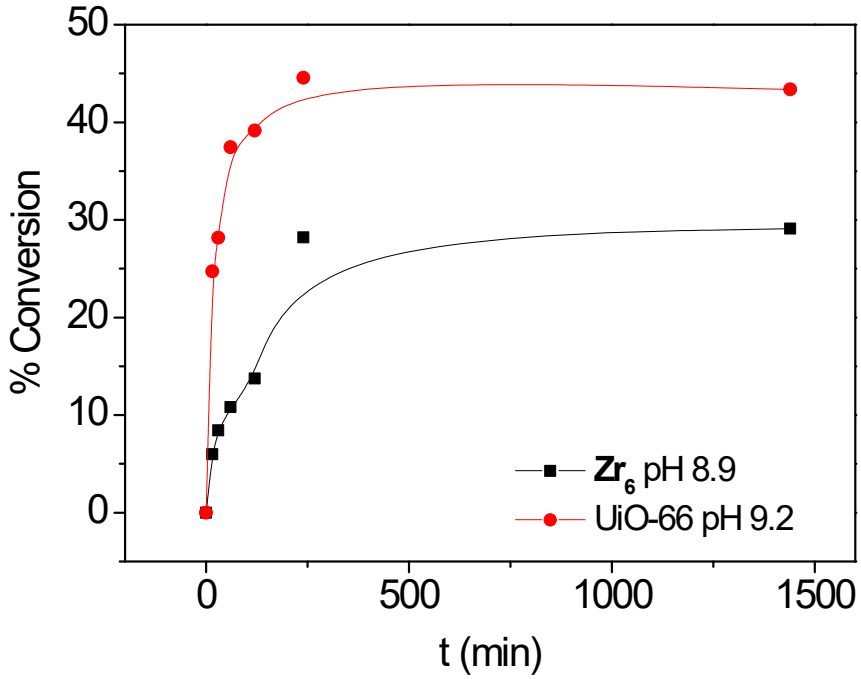

Figure S17. Catalyzed hydrolysis of **1** by UiO-66 , $\mathbf{Zr_6}$ in TRIS (0.1 mol L^{-1} – pH 9.8). Conditions: [MOF] = [$\mathbf{Zr_6}$] = 1.5 µmol; [**1**] = 25 µmol; 60ºC.

3.5 Computational speciation analysis

A computational speciation analysis was conducted to determine the molecular structure of the active species of the catalyst in aqueous solution. Previous characterization of the present **Zr_6** catalyst[2] suggested the presence of multiple **Zr_6** clusters differing in the number and nature of terminal ligands, combining chloride and aqua/hydroxo ligands. The most abundant species was found to be consistent with that bearing three chloride and two aqua ligands: $[Zr_6O_4(OH)_4(CH_3CO_2)_8(H_2O)_2Cl_3]^+$ (**Zr_6**) labeled as **Zr_6-Cl_3** from now on. Dissolving **Zr_6-Cl_3** in water triggers a sequence of thermodynamically favorable hydration and deprotonation steps depicted in **Scheme S2**. The initial hydration step (from **Zr_6-Cl_3** to **Zr_6-Cl_3'**, via the coordianation of two water molecules) was assumed in aqueous solution to saturate the coordination sphere of Zr(IV) ions with the number of ligands that they display in Zr-based MOFs. Next, the chloride ligands are replaced by water molecules, which spontaneously dissociate to form terminal hydroxo ligands through acid-base processes governed by very low pK_a values that vary between -0.45 and 1.03 (**Scheme S2**). This leads to the formation of the chloride-free, neutral **Zr_6-$(OH)_4$** species and is the reason for the resulting acidic pH, as discussed in the main text. The distribution of protons in the latter is consistent with the most stable configuration of 8-fold coordinated **Zr_6** nodes in Zr-based MOFs.[21]

According to our computational predictions, forming **Zr_6-$(OH)_4$** upon dissolving the putative **Zr_6-Cl_3** structure in water would lower the pH of the solution down to 2.23 (see **Table S4**, entry 1), which is too low as compared to the experimentally measured pH of 3.0. Similarly, assuming that the parent species is not the cationic **Zr_6-Cl_3** but its neutral **Zr_6-Cl_3-OH** counterpart leads to a too acidic solution with a pH of 2.35 (**Table S4**, entry 2). On the other hand, assuming that the original salt is exclusively composed by **Zr_6-$(OH)_4$**, which molecular mass is also consistent with the most intense peaks in the MS spectrum,[2] would lead to a slightly too high solution pH of 3.37 (3.22 when using equilibrium constants derived from experimental pK_a values to build the speciation model). A pH value of 3.0 is only obtained when mixtures of different species are considered to be present in the solvated **Zr_6**

material (see entries 4 and 5 of **Table S4**), further supporting that several ligand patterns coexist in the as-synthesized catalyst, explaining the complexity of the MS spectra obtained from analysis of **Zr_6** powders.[2] Most importantly, **Zr_6-$(OH)_4$** was found to systematically come up as the most abundant species when chemical equilibrium is reached at pH ≈ 3.0, regardless the examined composition of the dissolved catalytic material.

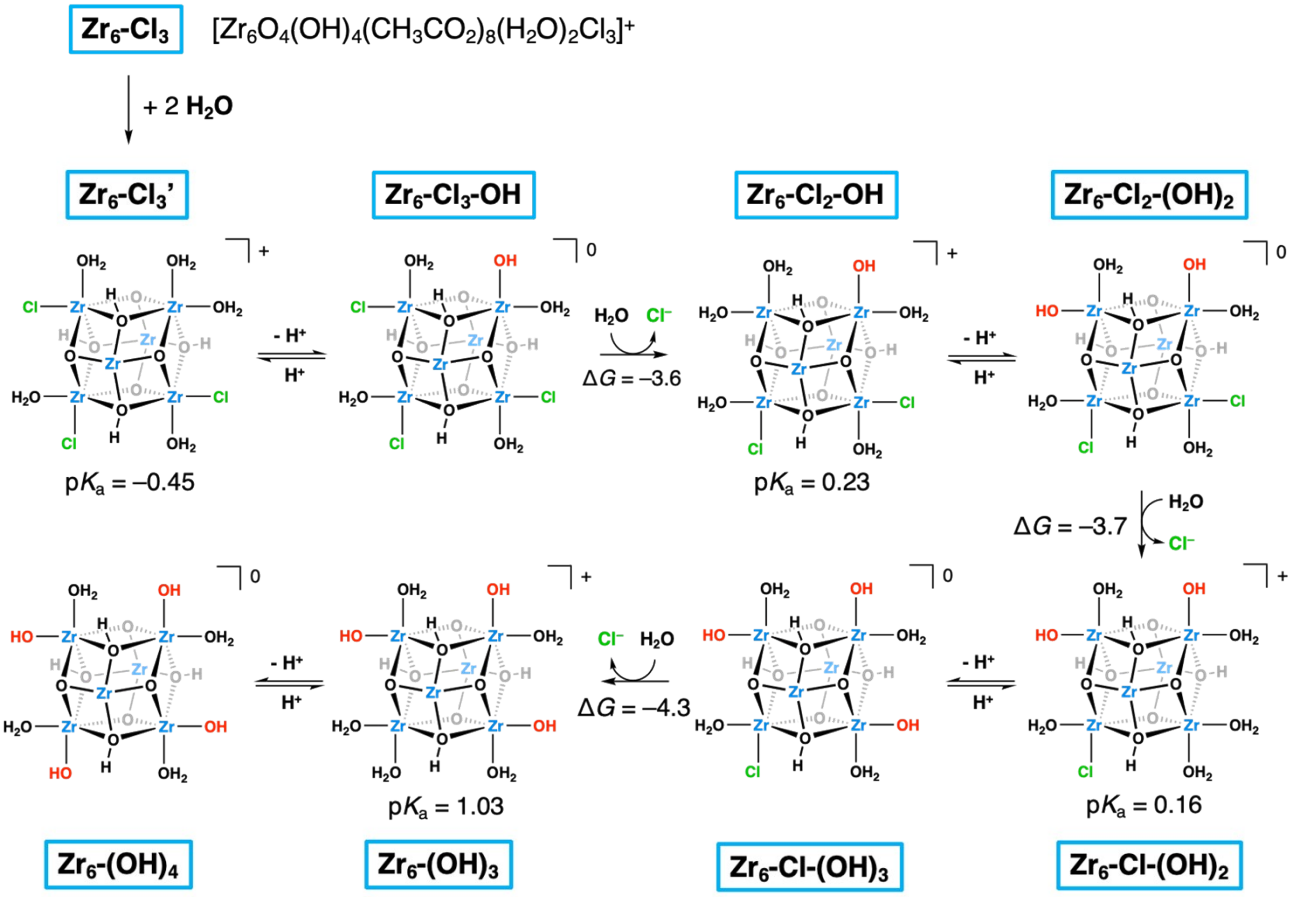

Scheme S2. Successive hydration and acid-base processes that the **Zr_6-Cl_3** cluster can undergo upon dissolution in water. Reaction Gibbs free energies for steps involving the replacement of a chloride by an aqua ligand are given in kcal mol^{-1}. pK_a Values were estimated following the procedure described in the Computational Details section. Zr-bound ligands highlighted in red indicate sites that have been deprotonated in previous acid-base equilibria.

This scenario, where **Zr_6-$(OH)_4$** is the most abundant species is supported by a potentiometric titration of **Zr_6** aqueous solution, suggesting three distinct pK_a values at p$K_{a\text{-}1}$ = 3.4, p$K_{a\text{-}2}$ = 4.8 and p$K_{a\text{-}3}$ =7.4 (Figure 6a, main text). Notably, the pK_a values for acid-base processes involving further deprotonation of **Zr_6-$(OH)_4$** (Figure 6b) were computationally estimated to be 3.80, 4.76 and 6.43, which are in very

good agreement with the experimental values. Previous studies on Zr-MOFs, postulated that the three corresponding deprotonations correspond to the μ_3-OH bridge (pK_{a1}), and the water ligand coordinated to the Zr^{IV} (pK_{a2} 4.8 and pK_{a3} 7.4).[22] However, as shown in **Scheme S3**, our DFT calculations indicate that protons from terminal aqua ligands of **Zr_6** are in all cases more acidic than μ_3-OH protons by ca. 7-11 kcal mol^{-1}. In fact, a recent computational study on the Brönsted acidity of Zr_6 nodes of the UiO-66 also proposed that μ_1-OH_2 protons are more acidic than μ_3-OH ones.[23] Thus, there are strong indications that the neutral **Zr_6-(OH)$_4$** cluster represents the active species of the catalyst at pH 3.0, while anionic species generated upon protolysis of terminal aqua ligands (**Zr_6-(OH)$_5$**, **Zr_6-(OH)$_6$** and **Zr_6-(OH)$_7$**, Figure 6b) are responsible for the catalysis when the pH is adjusted to higher values.

Table S4. Calculated solution pH and concentrations of the three major Zr_6-based species at chemical equilibrium by iterative application of equilibrium constant equations. Values in parentheses correspond to those calculated using the experimental K_a values for equilibria established between **Zr_6-(OH)$_4$**, **Zr_6-(OH)$_5$**, **Zr_6-(OH)$_6$** and **Zr_6-(OH)$_7$** species (see Scheme S2 for details).

Initial concentration (mol L^{-1})[a]			**Concentration at equilibrium (mol L^{-1})**			
Zr_6-Cl_3	**Zr_6-Cl_3-OH**	**Zr_6-(OH)$_4$**	**Zr_6-(OH)$_3$ (q = 1+)**	**Zr_6-(OH)$_4$ (q = 0)**	**Zr_6-(OH)$_5$ (q = 1-)**	**$pH_{equil.}$**
1.5×10^{-3}	-	-	$8.76\ (8.53) \times 10^{-5}$	$1.38\ (1.33) \times 10^{-3}$	$3.67\ (8.77) \times 10^{-5}$	2.23 (2.22)
-	1.5×10^{-3}	-	$6.65\ (6.43) \times 10^{-5}$	$1.38\ (1.32) \times 10^{-3}$	$4.90\ (11.5) \times 10^{-5}$	2.35 (2.34)
-	-	1.5×10^{-3}	$4.94\ (5.83) \times 10^{-6}$	$1.08\ (0.90) \times 10^{-3}$	$4.00\ (5.84) \times 10^{-4}$	3.37 (3.22)
2.0×10^{-4}	-	1.3×10^{-3}	$1.37\ (1.39) \times 10^{-5}$	$1.28\ (1.11) \times 10^{-3}$	$2.03\ (3.75) \times 10^{-4}$	3.00 (2.93)
	2.0×10^{-4}	1.3×10^{-3}	$1.12\ (1.16) \times 10^{-5}$	$1.25\ (1.07) \times 10^{-3}$	$2.37\ (4.16) \times 10^{-4}$	3.08 (2.99)

[a] Besides these initial concentrations for Zr_6-based clusters, the following non-zero initial concentrations were set: $[H^+]_0 = [OH^-]_0 = 10^{-7}$ and $[H_2O]_0 = 55.5$ mol L^{-1}, which were used to account as well for water self-ionization processes.

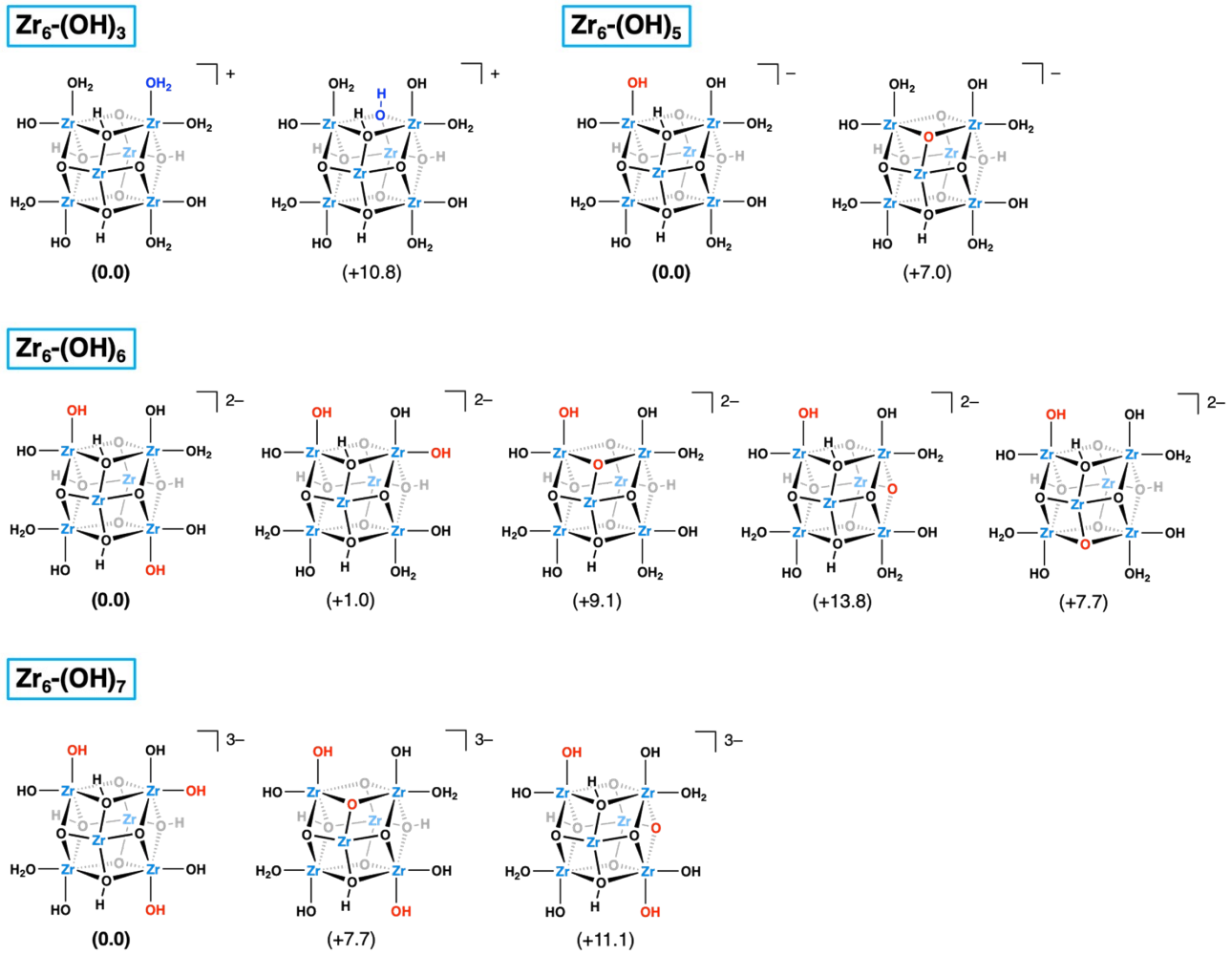

Scheme S3. Relative Gibbs free energies (kcal mol^{-1}) for structural isomers of Zr_6 with different protonation states. Note that the reference structure for the analysis of each species corresponds to the most stable configuration of the system containing one more proton. That is, to investigate the isomerism of **Zr_6-(OH)$_6$**, we have started from the most stable isomer of **Zr_6-(OH)$_5$** and so forth.

3.6 Isotopic effect

To probe whether the reaction proceeds through a general base catalysis mechanism, or through an intramolecular pathway, the hydrolysis reaction was conducted using deuterated solvents. For general base mechanisms, the catalyst activates a water molecule of the solvent which acts as the nucleophile for the hydrolysis of **1**. In contrast, in the intramolecular mechanism the hydrolytic attack is promoted by the catalyst itself. As D_2O is less labile than H_2O, the general base mechanism is more affected by the solvent changes, generally shows a slower kinetics in conditions using deuterated solvents.[24]

No acidification was observed after cluster addition when the reactions were conducted in deuterated solvents. Thus, the pD was corrected to 2.7 using a commercial DCl solution (35% wt) for the reaction in D_2O, while a HEPES buffer of pD 6.2 was especially prepared for the reaction in this condition (see details on General Remarks) in order to ensure reactions in both deuterated and protic solvents were carried out in the same conditions. The reactions were followed for 24 h. After this time, the pD dropped to 1.9 and 4.7, like observed for reactions using regular aqueous conditions.

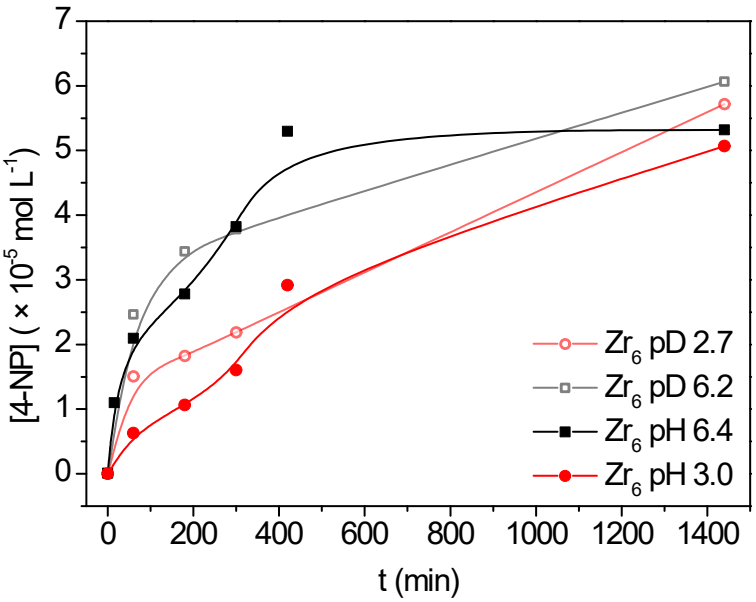

Figure S18. Comparison of Zr_6-catalyzed hydrolysis of **1** using regular and deuterated solvents. Conditions: [Zr_6] = 1.5 µmol; [1] = 25 µmol; 60ºC; in water (1 mL - pH 3.0); in HEPES 0.1 mol L^{-1} - pH 7.0 (1 mL – pH 6.4); in deuterium (1 mL - pD 2.7); in HEPES, 0.1 mol L^{-1} – pD 6.4 (1 mL - pD 6.2.

As no significant difference was found between the reactions conducted in deuterated or regular solvents, the mechanism likely follows an intramolecular pathway.

3.7 Additional computational results

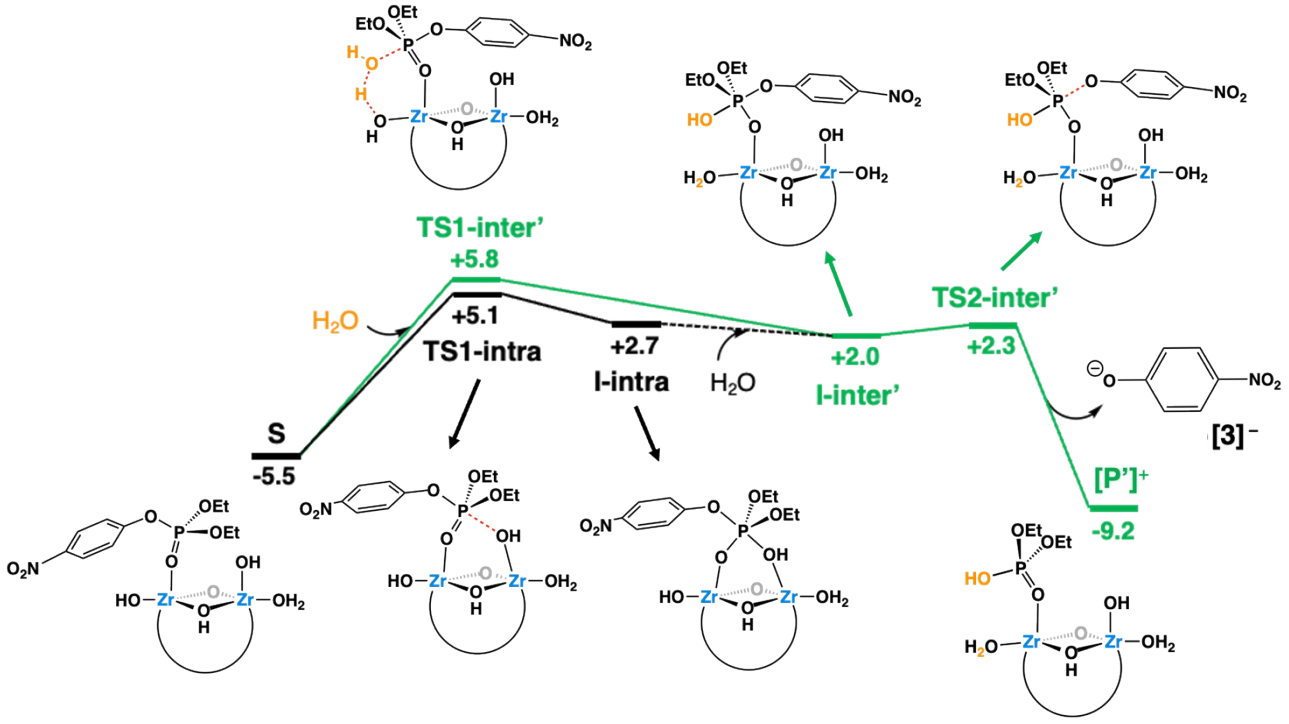

Figure S19. Gibbs free-energy profile (kcal mol^{-1}) for the hydrolysis of **1** catalyzed by **Zr_6-$(OH)_4$** through alternative reaction mechanisms.

Owing to the small free-energy difference between **TS1-intra** and **TS1-inter'** (0.7 kcal mol^{-1}), it is not possible to rule out that a minor part of the reaction proceeds through the *inter'* path (green lines). Also, the incorporation of an aqua ligand to **I-intra**, followed by a proton rearrangement would cause the *intra* (black) and the *inter'* (green) path to converge at the **I-inter'** species, allowing to postulate a possible reaction pathway that goes through **TS1-intra** and **TS2-inter'**, the latter transition state being 3 kcal mol^{-1} lower in energy than **TS2** (Figure 7). However, analyzing the feasibility and kinetics of the **I-intra** to **I-inter'** transformation is rather complex and would not provide further valuable information, given that the relative free-energies of **TS1-intra** and **TS2** are very close, and therefore, the overall reaction barrier would remain practically unaltered.

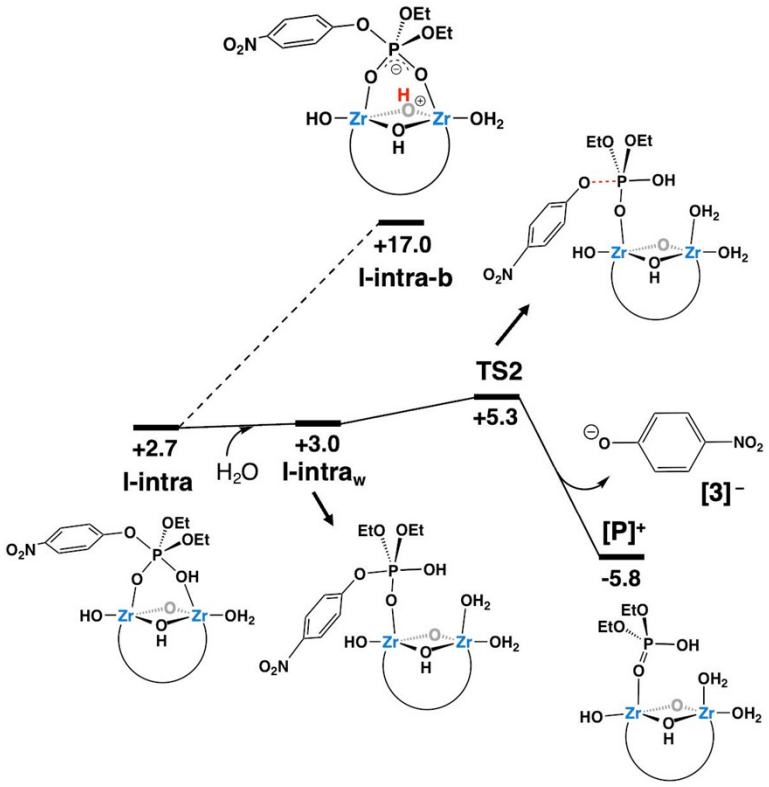

Figure S20. Comparison between the proposed mechansim to form the products from **I-intra** (solid lines) and an alternative path that is higher in energy, which involves the participation of a bridging oxygen of the cluster acting as a Brönsted base through **I-intra-b (**dashed lines).

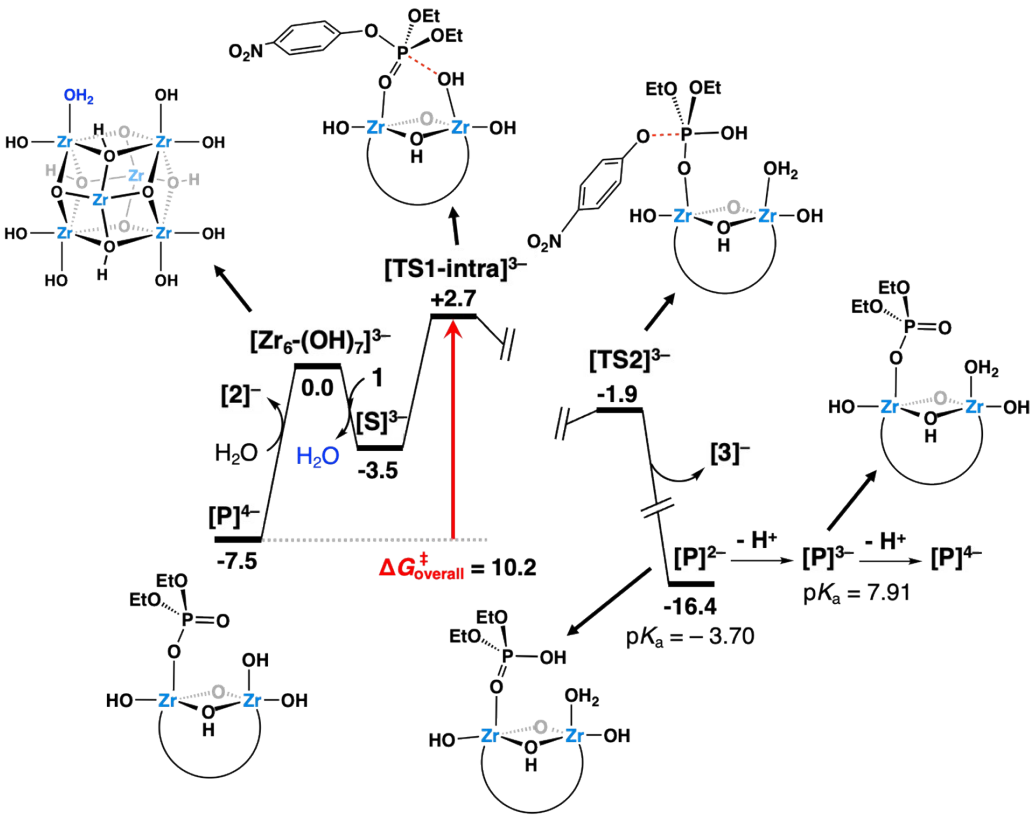

Figure S21. Gibbs free-energy profile (kcal mol^{-1}) for the hydrolysis of **1** catalyzed by **Zr_6-$(OH)_7$**, the most abundant form of the catalyst at pH 9. Intermediates between [**TS-intra**]$^{3-}$ and [**TS2**]$^{3-}$ were omitted.

As [**P**]$^{3-}$ was found to exhibit a pK_a of 7.91, [**P**]$^{4-}$ is expected to spontaneously form at the reaction pH of 9 and therefore, unlike in the reaction at pH 3 (Figure 9 in the main text), there is no energy cost associated to the generation of the species that releases the [**2**]$^{-}$ product. The [**TS-inter'**]$^{3-}$ (not shown in **Figure S21**) involved in the most favorable intermolecular mechanism was found to be at +5.2 kcal mol^{-1}, being higher in energy than [**TS-intra**]$^{3-}$, which lies at +2.7 kcal mol^{-1}.

Additional calculations were conducted to compare the stability of a set of configurations, covering both mono- and bidentate coordination modes for acetate ligands at pH 3, as well as their possible replacement by water molecules, yield acetic acid in solution through protolysis of one of these water molecules. As illustrated in **Scheme S4**, all the analyzed species lie within a very narrow range of free energy (< 2 kcal mol^{-1}), which falls inside the limits of computational uncertainty. Therefore, given the

labile nature of Zr(IV) ions, all species shown in **Scheme S4** might be postulated to co-exist in solution; thus, being not possible to rule out that ligand decoordination could occur to some extent.

However, and most importantly, this was found not to have a significant impact on the reaction barriers nor in the overall picture of the reaction mechanism. As shown in **Table S5**, the free-energy barriers for the nucleophilic attack step through the two most favorable pathways involving **TS1-intra** and **TS1-inter'**, respectively, are very similar for both the 6-fold acetate-coordinated model discussed in the manuscript and the 5-fold coordinated model shown in **Scheme S4** (rightmost structure), exhibiting differences of less than 2 kcal mol^{-1}. Moreover, the trend in the relative stability of transition states is preserved in the 5-fold coordinated model, supporting that the conclusions inferred from the 6-fold coordinated model are sound and still stand within a more sophisticated speciation scenario that considers changes in acetate ligands' coordination.

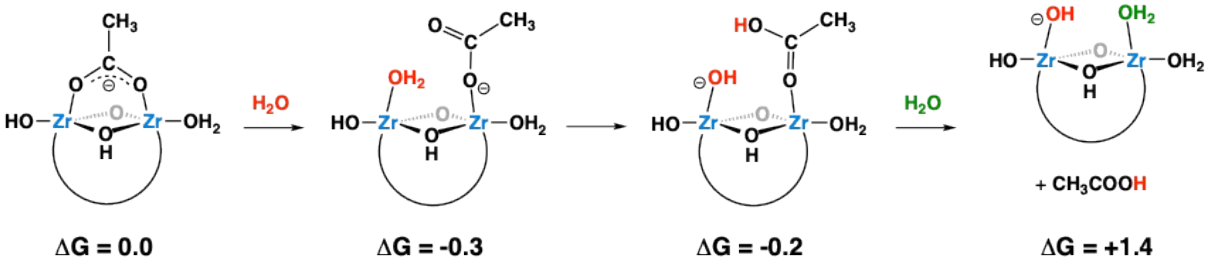

Scheme S4. Explored processes regarding the coordination of acetate ligands at pH 3. Relative Gibbs free energies (at 60 °C) for each of the species are given in kcal mol^{-1}.

Table S5. Comparison of free-energy barriers (kcal mol^{-1}) for the nucleophilic attack step through the two most likely pathways, calculated on 6- and 5-fold acetate-coordinated models of the Zr_6 cluster at pH 3.

Model	$\Delta G^{\ddagger}$ **(S→TS1-intra)**	$\Delta G^{\ddagger}$ **(S→TS1-inter')**
6-fold coordinated	10.6	11.3
5-fold coordinated (one missing acetate)	8.8	12.1

4 Computational Details

4.1 General procedure

DFT calculations were carried out using the Gaussian 16 (rev. A01) code.[25] The geometries of all systems were fully optimized without any symmetry constraints at the B3LYP-D3BJ level[26–30] using the 6-31G(d,p) basis set[31–33] for main group elements and the LANL2DZ basis set[34] supplemented by Frenking's f-type polarization functions[35] for Zr atoms. Solvent effects of water were included by means of the IEF-PCM solvent model[36] as implemented in Gaussian 16. The minimum or saddle-point nature of all species was confirmed via frequency calculation. Electronic energies were corrected by performing a single point calculation on optimized structures using a more extended triple-ζ basis set (LANL2TZ(f)[35,37] for Zr and 6-311G(d,p)[38] for the remaining elements). Free energies were calculated at the standard concentration of 1 mol/L at 60 °C using the GoodVibes code,[39] except those used to build the speciation model, which were obtained using a temperature of 25 °C. Free-energy variations associated to displacing acid-base equilibria (ΔG) were estimated through equation 2:

Equation 2: $\Delta G = \Delta G_r^{(1M,\ 60\ °C)} - \delta G_{H^+}^{(1atm,\ 60\ °C\ à\ 1M,\ 60\ °C)} + \delta G_{H^+}^{(1atm,\ 60\ °C\ à\ nM,\ 60\ °C)}$

where $\Delta G_r^{(1M,\ 60\ °C)}$ is the deprotonation free-energy obtained from the pK_a by means of equation 3, and $\delta G_{H^+}^{(1atm,\ 60\ °C\ à\ nM,\ 60\ °C)}$ accounts for the free-energy variation upon changing from a reference state of 1 atm at 60 ºC for protons to a different state that corresponds to their concentration (n) at the experimental pH.

Equation 3: $\Delta G_r^{(1M,\ 60\ °C)} = -\ln(10)\ RT\ pK_a$

Equation 4: $\delta G_{H^+}^{(1atm,\ 60\ °C\ à\ nM,\ 60\ °C)} = RT\ \ln(n\ RT)$

Thus, $\delta G_{H^+}^{(1atm,\ 60\ °C\ à\ 1M,\ 60\ °C)}$ was determined to be +2.19 kcal mol^{-1}, whereas $\delta G_{H^+}^{(1atm,\ 60\ °C\ à\ nM,\ 60\ °C)}$ takes values of -2.38 and -0.86 kcal mol^{-1} at pH 3 and 2, respectively.

A dataset collection of the optimized structures for the most relevant species is available in the ioChem-BD repository [40] and can be accessed via https://iochem-bd.urv.es/browse/handle/100/1190.

4.2 pK_a determination

Determining pK_a values with accuracy on the sole basis of computational data is still a bing challenge for computational chemistry due to the difficulties inherent to modelling protons in aqueous solution. To circumvent this issue, pK_a values for **Zr_6**-based species were estimated here as follows. First, we calculated the free energy differences between the set of inorganic acids compiled in **Table S6**, for which experimental pK_a values are available,[41] and their conjugated bases. These data were then fitted to a linear regression model, shown in **Figure S22**, which provides a linear equation to calculate pK_a values from free-energy differences between acids and their conjugated bases, circumventing thus the need of using any value for the free-energy of a proton in solution to calculate protonation free energies. Free energy differences between protonated and deprotonated **Zr_6** clusters were finally interpolated into the fitting represented in **Figure S22** to obtain the pK_a values discussed in the text.

Table S6. Compilation of experimentally-reported pK_a values for a series of inorganic acids and the calculated free-energy difference between them and their conjugated base.[a]

Acid	pK_a (exp.)[b]	$\Delta G_{acid\text{-}base}$ (kcal mol^{-1})
H_3PO_4	1.97	-279.40
H_3AsO_4	2.22	-283.08
HNO_2	3.29	-289.90
H_3AlO_3	11.2	-316.06
H_3AsO_3	9.22	-301.75
BrOH	8.70	-306.34
IOH	11.00	-308.82
H_4GeO_4	8.68	-300.97
H_3BO_3	9.23	-307.04
$HClO_3$	-1.00	-274.73
HNO_3	-1.30	-274.88
H_3GaO_3	10.32	-310.67
H_2SO_4	-3.00	-262.16
H_3PO_3	2.00	-291.69
H_2CO_3	6.37	-287.07

[a]All systems were fully optimized at the B3LYP-D3BJ level of theory using the LANL2TZ(f) basis set and pseudopotentials for heavy elements and the 6-311G(d,p) basis set for light elements. Solvent effects of water were included in through the IEF-PCM solvent model. [b]Data obtained from Williams (2022).[41]

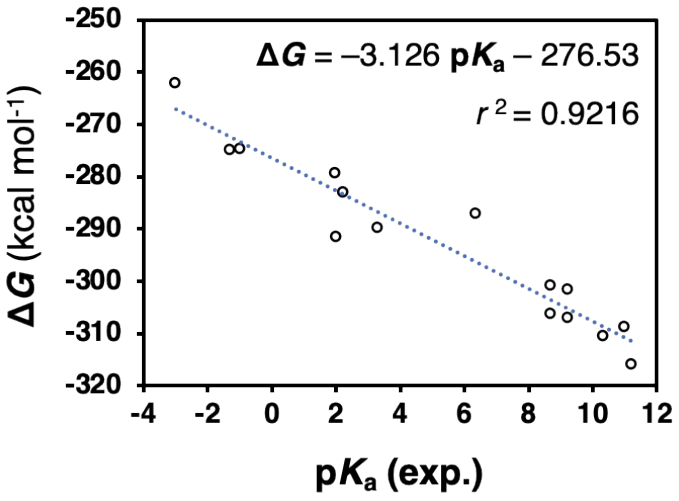

Figure S22. Linear fitting of the DFT-derived protonation free-energies (ΔG) for the inorganic acids listed in Table S5 against their experimental pK_a values. ΔG values were calculated as the free-energy difference between every acid and its conjugated base, as follows: $\Delta G = G_{acid} - G_{base}$.

5 References

1 P. K. Glasoe and F. A. Long, *J. Phys. Chem.*, 1960, **64**, 188–190.

2 S. Dai, C. Simms, I. Dovgaliuk, G. Patriarche, A. Tissot, T. N. Parac-Vogt and C. Serre, *Chem. Mater.*, 2021, **33**, 7057–7066.

3 M. Puchberger, F. R. Kogler, M. Jupa, S. Gross, H. Fric, G. Kickelbick and U. Schubert, *Eur. J. Inorg. Chem.*, 2006, **2006**, 3283–3293.

4 Y. Zhang, F. de Azambuja and T. N. Parac-Vogt, *Catal. Sci. Technol.*, 2022, **12**, 3190–3201.

5 D. Van den Eynden, R. Pokratath, J. P. Mathew, E. Goossens, K. De Buysser and J. De Roo, *Chem. Sci.*, 2023, **14**, 573–585.

6 Y. Zhang, I. Y. Kokculer, F. de Azambuja and T. N. Parac-Vogt, *Catal. Sci. Technol.*, 2023, **13**, 100–110.

7 H. Noh, C.-W. Kung, T. Islamoglu, A. W. Peters, Y. Liao, P. Li, S. J. Garibay, X. Zhang, M. R. DeStefano, J. T. Hupp and O. K. Farha, *Chem. Mater.*, 2018, **30**, 2193–2197.

8 F. de Azambuja, A. Loosen, D. Conic, M. van den Besselaar, J. N. Harvey and T. N. Parac-Vogt, *ACS Catal.*, 2021, **11**, 7647–7658.

9 A. Loosen, F. de Azambuja, S. Smolders, J. Moons, C. Simms, D. De Vos and T. N. Parac-Vogt, *Chem. Sci.*, 2020, **11**, 6662–6669.

10 R. C. Klet, Y. Liu, T. C. Wang, J. T. Hupp and O. K. Farha, *J Mater Chem A*, 2016, **4**, 1479–1485.

11 G. Aquilanti, M. Giorgetti, R. Dominko, L. Stievano, I. Arčon, N. Novello and L. Olivi, *J. Phys. Appl. Phys.*, 2017, **50**, 074001.

12 A. Filipponi and A. Di Cicco, *Phys. Rev. B*, 1995, **52**, 15135–15149.

13 A. Filipponi, A. Di Cicco and C. R. Natoli, *Phys. Rev. B*, 1995, **52**, 15122–15134.

14 J. Chu, F.-S. Ke, Y. Wang, X. Feng, W. Chen, X. Ai, H. Yang and Y. Cao, *Commun. Chem.*, 2020, **3**, 5.

15 Y. Zhang, F. de Azambuja and T. N. Parac-Vogt, *Coord. Chem. Rev.*, 2021, **438**, 213886.

16 Y. Liao, T. R. Sheridan, J. Liu, Z. Lu, K. Ma, H. Yang, O. K. Farha and J. T. Hupp, *ACS Catal.*, 2024, **14**, 437–448.

17 V. M. Jayasinghe-Arachchige, L. F. Serafim, Q. Hu, C. Ozen, S. N. Moorkkannur, G. Schenk and R. Prabhakar, *ACS Catal.*, 2023, **13**, 3131–3147.

18 D. J. Kennedy, B. P. Mayer, S. E. Baker and C. A. Valdez, *Inorganica Chim. Acta*, 2015, **436**, 123–131.

19 L. V. Penkova, A. Maciąg, E. V. Rybak-Akimova, M. Haukka, V. A. Pavlenko, T. S. Iskenderov, H. Kozłowski, F. Meyer and I. O. Fritsky, *Inorg. Chem.*, 2009, **48**, 6960–6971.

20 D. Yang, M. A. Ortuño, V. Bernales, C. J. Cramer, L. Gagliardi and B. C. Gates, *J. Am. Chem. Soc.*, 2018, **140**, 3751–3759.

21 N. Planas, J. E. Mondloch, S. Tussupbayev, J. Borycz, L. Gagliardi, J. T. Hupp, O. K. Farha and C. J. Cramer, *J. Phys. Chem. Lett.*, 2014, **5**, 3716–3723.

22 R. C. Klet, Y. Liu, T. C. Wang, J. T. Hupp and O. K. Farha, *J. Mater. Chem. A*, 2016, **4**, 1479–1485.

23 H. Chen, *Chem. Phys. Lett.*, 2022, **800**, 139658.

24 K. A. Deal, A. C. Hengge and J. N. Burstyn, *J. Am. Chem. Soc.*, 1996, **118**, 1713–1718.

25 Frisch, M. J.; Trucks, G. W.; Schlegel, H. B.; Scuseria, G. E.; Robb, M. A.; Cheeseman, J. R.; Scalmani, G.; Barone, V.; Petersson, G. A.; Nakatsuji, H.; Li, X.; Caricato, M.; Marenich, A. V.; Bloino, J.; Janesko, B. G.; Gomperts, R.; Mennucci, B.; Hratchian, H. P.; Ortiz, J. V.; Izmaylov, A. F.; Sonnenberg, J. L.; Williams; Ding, F.; Lipparini, F.; Egidi, F.; Goings, J.; Peng, B.; Petrone, A.; Henderson, T.; Ranasinghe, D.; Zakrzewski, V. G.; Gao, J.; Rega, N.; Zheng, G.; Liang, W.; Hada, M.; Ehara, M.; Toyota, K.; Fukuda, R.; Hasegawa, J.; Ishida, M.; Nakajima, T.; Honda, Y.; Kitao, O.; Nakai, H.; Vreven, T.; Throssell, K.; Montgomery Jr., J. A.; Peralta, J. E.; Ogliaro, F.; Bearpark, M. J.; Heyd, J. J.; Brothers, E. N.; Kudin, K. N.; Staroverov, V. N.; Keith, T. A.; Kobayashi, R.; Normand, J.; Raghavachari, K.; Rendell, A. P.; Burant, J. C.; Iyengar, S. S.; Tomasi, J.; Cossi, M.; Millam, J. M.; Klene, M.; Adamo, C.; Cammi, R.; Ochterski, J. W.; Martin, R. L.; Morokuma, K.; Farkas, O.; Foresman, J. B.; Fox, D. J., Gaussian 16 Rev. A.03 (version Wallingford, CT) Wallingford, CT, 2016, Wallingford, CT. 2016.

26 C. Lee, W. Yang and R. G. Parr, *Phys. Rev. B*, 1988, **37**, 785–789.

27 A. D. Becke, *J. Chem. Phys.*, 1993, **98**, 5648–5652.

28 P. J. Stephens, F. J. Devlin, C. F. Chabalowski and M. J. Frisch, *J. Phys. Chem.*, 1994, **98**, 11623–11627.

29 S. Grimme, J. Antony, S. Ehrlich and H. Krieg, *J. Chem. Phys.*, 2010, **132**, 154104.

30 S. Grimme, S. Ehrlich and L. Goerigk, *J. Comput. Chem.*, 2011, **32**, 1456–1465.

31 W. J. Hehre, R. Ditchfield and J. A. Pople, *J. Chem. Phys.*, 2003, **56**, 2257–2261.

32 P. C. Hariharan and J. A. Pople, *Theor. Chim. Acta*, 1973, **28**, 213–222.

33 M. M. Francl, W. J. Pietro, W. J. Hehre, J. S. Binkley, M. S. Gordon, D. J. DeFrees and J. A. Pople, *J. Chem. Phys.*, 1982, **77**, 3654–3665.

34 P. J. Hay and W. R. Wadt, *J. Chem. Phys.*, 1985, **82**, 299–310.

35 A. W. Ehlers, M. Böhme, S. Dapprich, A. Gobbi, A. Höllwarth, V. Jonas, K. F. Köhler, R. Stegmann, A. Veldkamp and G. Frenking, *Chem. Phys. Lett.*, 1993, **208**, 111–114.

36 E. Cancès, B. Mennucci and J. Tomasi, *J. Chem. Phys.*, 1997, **107**, 3032–3041.

37 L. E. Roy, P. J. Hay and R. L. Martin, *J. Chem. Theory Comput.*, 2008, **4**, 1029–1031.

38 R. Krishnan, J. S. Binkley, R. Seeger and J. A. Pople, *J. Chem. Phys.*, 2008, **72**, 650–654.

39 G. Luchini, R. Paton, J. Alegre-Requena, J. Rodríguez-Guerra, E. Berquist, J. Chen, IFunes, J. Velmiskina, froessler, H. Mayes, S. S. S. Vejaykummar and sibo, patonlab/GoodVibes Zenodo 2022.

40 M. Álvarez-Moreno, C. De Graaf, N. López, F. Maseras, J. M. Poblet and C. Bo, *J. Chem. Inf. Model.*, 2015, **55**, 95–103.

41 R. Williams, pKa data compiled by R. Williams, https://organicchemistrydata.org/hansreich/resources/pka/pka_data/pka-compilation-williams.pdf, (accessed September 2, 2023).